CHAPTER 4

RESULTS AND DISCUSSION

This chapter describes about results and discussion of the experiments which were done in chapter 3. They are gas flow rate, Rutherford backscattering spectrometer, film thickness, mass increase, density increase, x-ray diffractometer, energy dispersive x-ray, scanning electron microscopy, microhardness test and wear test.

4.1 Gas Flow Rate

Figure 4.1 shows the plot of log F versus log ΔH for NH_3, Ar and C_2H_2. It has found that the correlation between log F and log ΔH follows the linear equation.

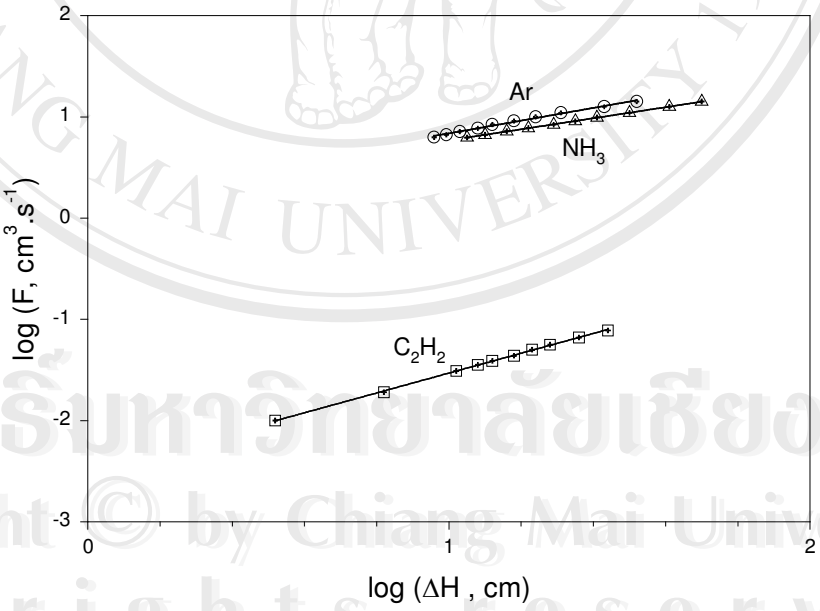

Figure 4.1 Log F versus log ΔH of NH_3, Ar and C_2H_2.

The equations, calculated ΔH and r^2 at the specified flow rate are shown in Table 4.1.

Table 4.1 The equations, calculated ΔH and r^2 for NH_3, Ar and C_2H_2.

Gases	Equations	r^2	Testing flow rate ($cm^3.s^{-1}$)	ΔH (cm)
NH_3	$\log F = 0.545 \log \Delta H + 0.223$.	1.00	10.0	26.6
Ar	$\log F = 0.628 \log \Delta H + 0.208$,	0.992	9.99	18.2
			9.97	18.2
			9.95	18.1
C_2H_2	$\log F = 0.980 \log \Delta H - 2.51$,	0.999	0.01	3.3
			0.03	10.2
			0.05	17.1

4.2 Rutherford Backscattering Spectrometer

4.2.1 Nitridation by Direct Metal-Gas Reaction

RBS spectra of MJ12 and MJ47 without and with 1000-1300 K nitridation are shown in Figure 4.2. Ti and Al were detected indicating that these elements are the majorities containing in the alloys. Nb was detected only in the as-received alloys. Atomic masses of Cr and Mn are about the same as that of Ti and concentration of Ti in the alloys is much higher than those of Cr and Mn. Therefore, the spectra for Ti, Cr and Mn are mingled leading to the undetection of Cr and Mn. There were no detection of B and N. These light elements have low scattering cross-section. After nitridation, RBS spectra of the alloys deviate from the as-received. This show that dissolution of N resulting in deviation of the alloy surface composition from the original.

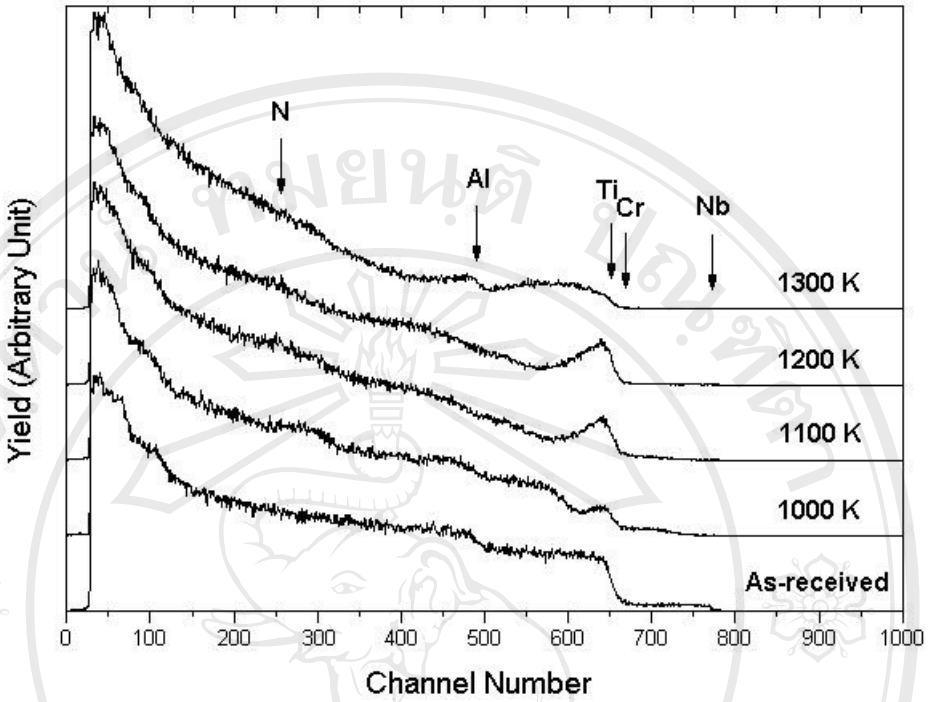

(a)

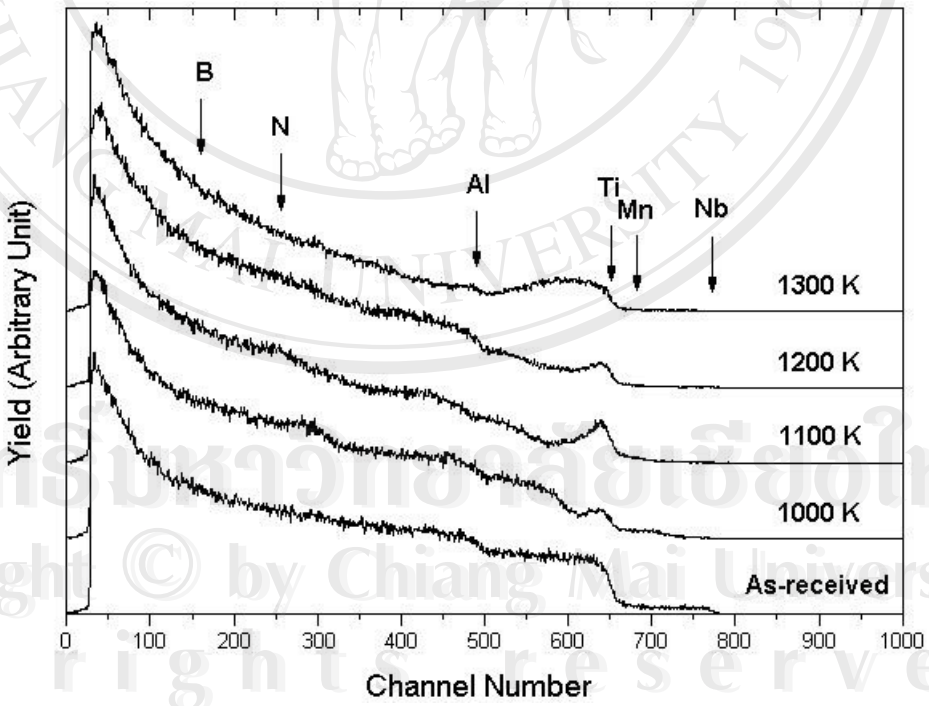

(b)

Figure 4.2 RBS spectra of (a) MJ12 and (b) MJ47 before and after nitridation by direct metal-gas reaction.

4.2.2 Carburization by Directly Applying Voltages

RBS spectra of MJ12 and MJ47 before and after carburization are shown in Figure 4.3. Before carburization, Ti, Al and Nb were detected but there were no detection of Cr, Mn and B. After carburization, Ti and C were detected on both alloys. Although C is a light element, its signal coming from C-riched regions was strong enough to be detected. They are the solid C deposited on the alloy surfaces.

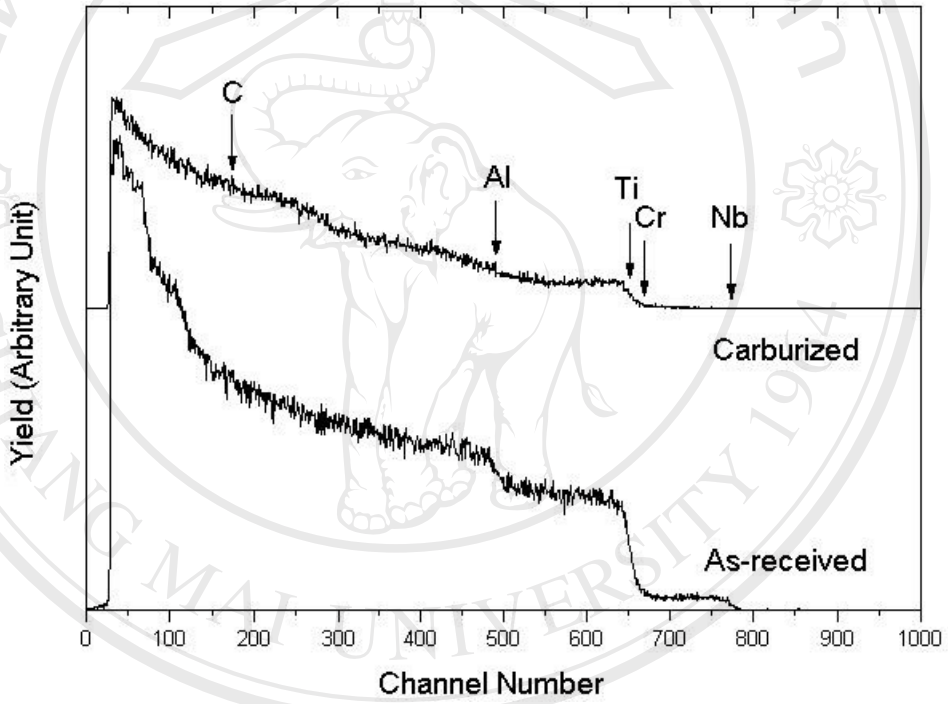

(a)

(Figure is continued to next page.)

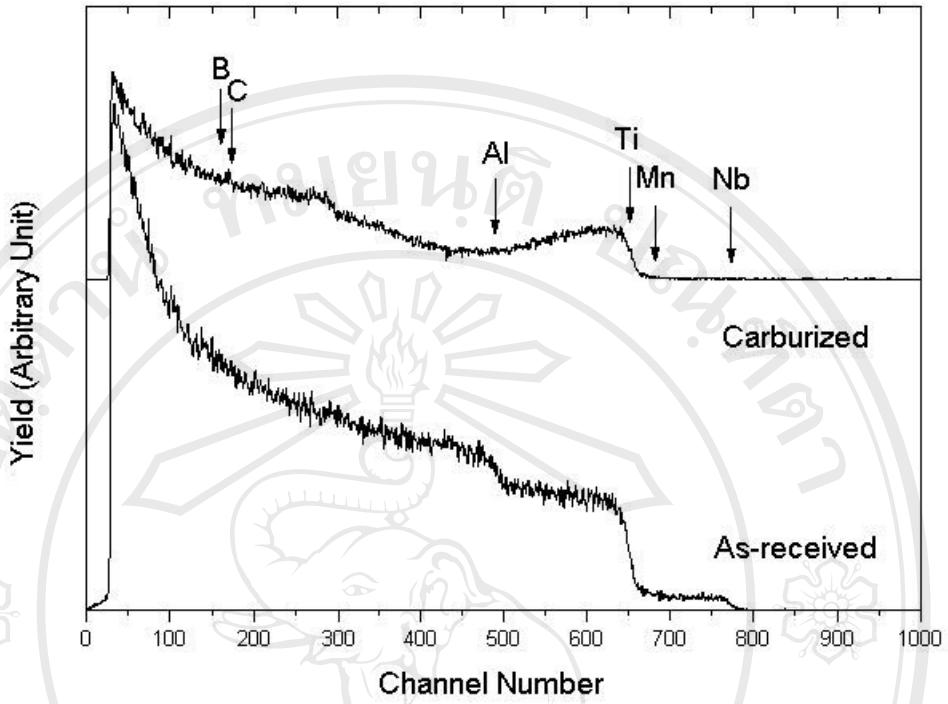

(b)

Figure 4.3 RBS spectra of (a) MJ12 and (b) MJ47 before and after carburization by directly applying voltages.

4.3 Film Thickness, Mass Increase and Density Increase

4.3.1 Nitridation by Direct Metal-Gas Reaction

The nitride thickness (d), mass increase (Δm) and density increase ($\Delta \rho$) for MJ12 and MJ47 with 1000-1300 K nitridation are shown in Figure 4.4. It is evident that they are increased with the nitridation temperature. The effect of temperature on diffusion coeffient of N in TiAl alloys can be explained by considering the jump frequency of N atom. During the nitridation process, some nitrogen diffused and dissolved in the alloy matrices. N atom occupied the interstitial site in FCC structure of TiAl alloy [34] as shown in Figure 4.5. The jump frequency of atom in the interstitial site to the nearest neighbor interstitial site (ω) can be expressed as

$$\omega = \tilde{\nu} \exp(-\frac{\Delta G^m}{kT}), \qquad [35]$$

where $\tilde{\nu}$ is a vibration frequency, ΔG^m is Gibbs free energy of migration, k is Boltzmann's constant and T is absolute temperature. It is clear that the jump frequency increase with the increasing temperature. The diffusion coefficient for the interstitial solid solution is given by

$$D = \beta\omega a^2, \qquad [36]$$

where β is geometric factor which depends on the structure and on the type of interstitial site and a is lattice parameter. This shows that the diffusion coefficient increase with the increasing of jump frequency. Solution for diffusion in this study is

$$\frac{c - c_s}{c_0 - c_s} = erf\left(\frac{x}{2\sqrt{Dt}}\right), \qquad [37]$$

where c is concentration of solute at any depth x and time t, c_s is concentration of solute at materials surface, c_0 is concentration of solute in matrix at $t = 0$ and *erf* means the error function. In this study, $c_0 = 0$. Thus

$$\frac{c}{c_s} = 1 - erf\left(\frac{x}{2\sqrt{Dt}}\right).$$

If we consider the depth at concentration equals to 10% of the surface concentration to be the film-substrate interface, then we have

$$\frac{x}{2\sqrt{Dt}} \approx 1$$

and

$$x^2 \approx 4Dt.$$

This shows that layer growth obeys the parabolic law. In this study, x represented by d which is nitride thickness and t is treatment time. Then we obtain

$$d^2 = 4Dt.$$

This shows that at constant time, the nitride thickness increase with the increasing diffusion coefficient. So, the nitride thickness would increase with the increasing temperature and corresponds to the experimental results.

The quantity of material which diffuses into the solid per unit area is

$$M(t) = 2c_s\sqrt{Dt/\pi}\ . \qquad [37]$$

The equation shows that $M(t)$ is increased with the increasing of D. The mass was increased with the increasing of temperature which corresponds to the experimental results. The density increase shows that the mass was increased with the increasing of temperature at higher rate than the thickness increase.

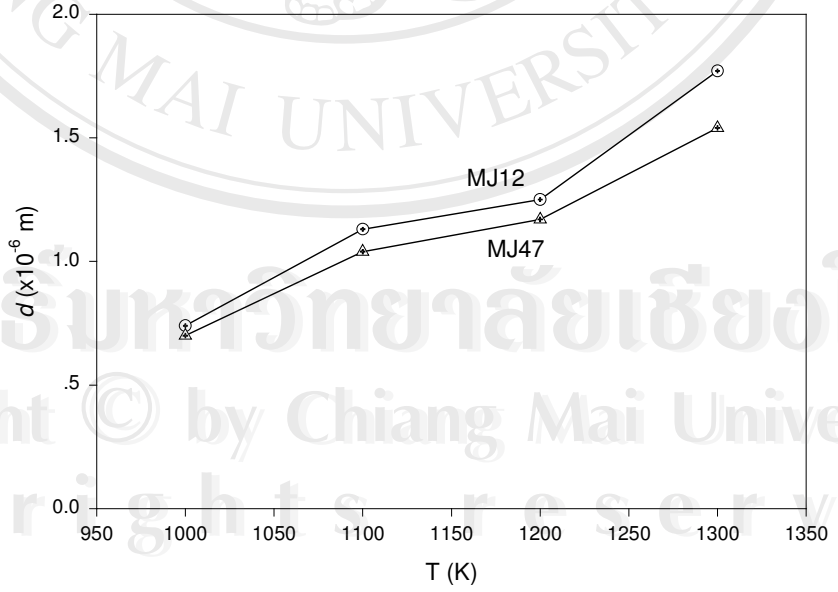

(a)

(Figure is continued to next page.)

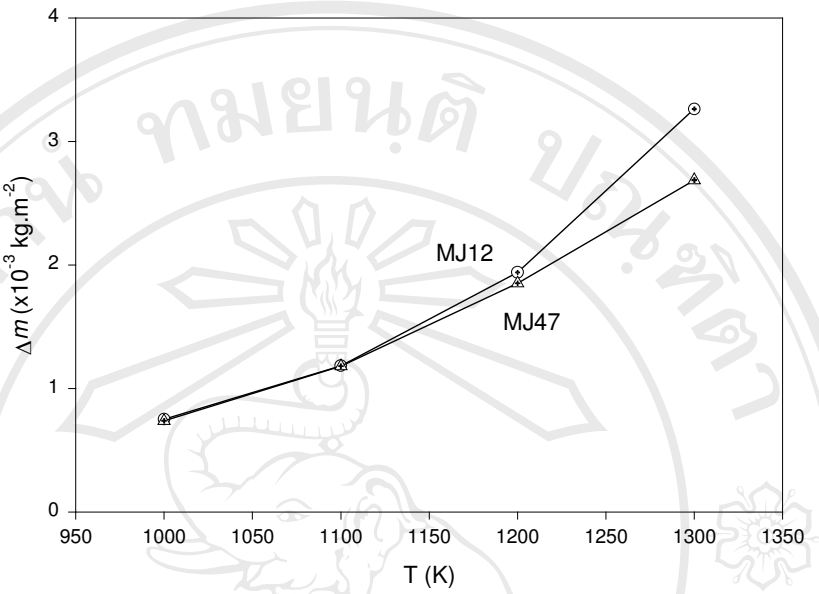

(b)

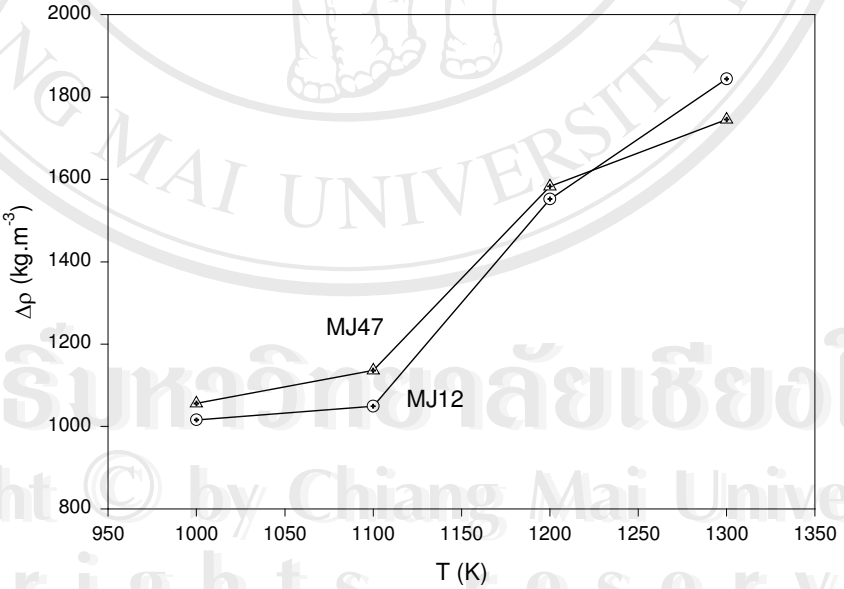

(c)

Figure 4.4 (a) Nitridation depth, (b) mass increase and (c) density increase of MJ12 and MJ47 with 1000–1300 K nitridation.

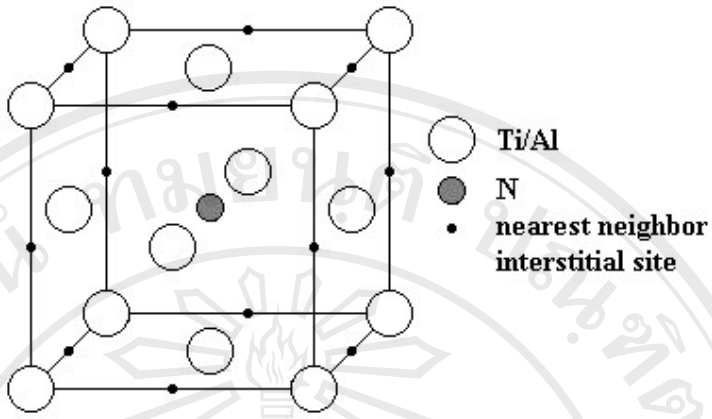

Figure 4.5 N atom in FCC structure of TiAl alloy.

Diffusion coefficient (*D*) for MJ12 and MJ47 with 1000-1300 K nitridation are shown in Figure 4.6. The results show that diffusion of N in MJ12 is faster than that in MJ47 and that nitride forming on MJ12 is better than that on MJ47. The Arrhenius type equation, the calculated activation energy (*Q*) and diffusion coefficient (*D*) for the diffusion of N in the two alloys are given in Table 4.2.

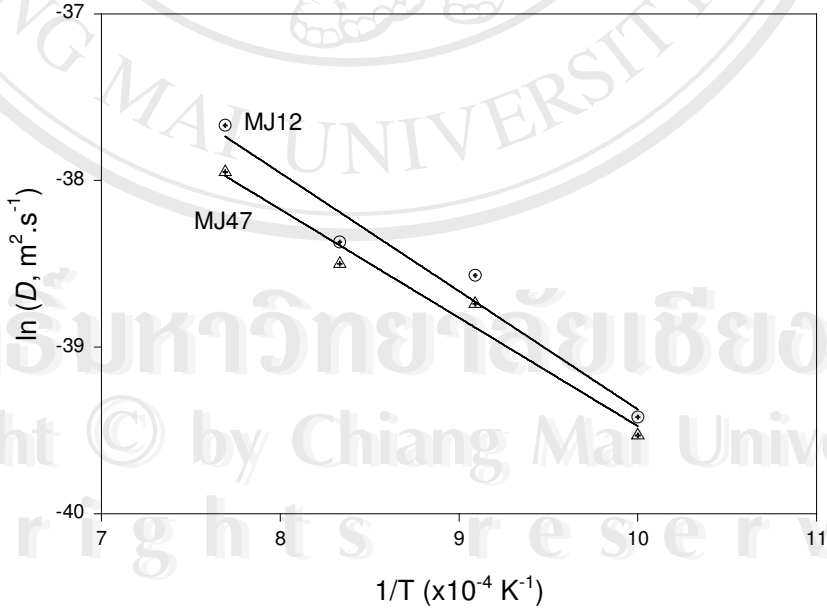

Figure 4.6 Diffusion coefficient for MJ12 and MJ47 with 1000–1300 K nitridation.

The activation energy is the energy required for nitrogen to penetrate across and dissolve in the alloy matrix. The results show that D of nitrogen in MJ12 is increased with the increasing temperature faster that in MJ47. In comparison with Q, 187.09 kJ.mol^{-1}, for nitrogen diffuses in Ti alloys reported by Sen [24], Q values for this study are lower. D reported by Sen [24] for temperature 1173-1273 K are 6.64×10^{-15} - 2.10×10^{-14} m^2.s^{-1}. D calculated in this study for temperature 1200-1300 K are 2.13×10^{-17} - 4.06×10^{-17} m^2.s^{-1}. D values for this study are lower. Ti alloys (HCP) and TiAl alloys (FCC) [10] microstructures, coating techniques, compositions and others are the factors to control N diffusion.

Table 4.2 Arrhenius type equation, calculated Q and D for MJ12 and MJ47.

Alloys	Equations	Q (kJ.mol^{-1})	D at 1000-1300 K (m^2.s^{-1})
MJ12	$\ln D = -7093/T - 32.28$ $D = 9.57\times10^{-15} \exp(-7093/T)$	58.97	7.89×10^{-18} - 4.06×10^{-17}
MJ47	$\ln D = -6504/T - 32.97$ $D = 4.80\times10^{-15} \exp(-6504/T)$	54.08	7.19×10^{-18} - 3.22×10^{-17}

4.3.2 Carburization by Directly Applying Voltages

The carbide thickness (d), mass increase (Δm) and density increase ($\Delta\rho$) for MJ12 and MJ47 with directly applying voltages are shown in Table 4.3. During the carburization process, carbon diffused and dissolved in the alloys. The diffusion of carbon in TiAl alloys is the interstitial mechanism [26]. During applying the voltages across carbon rods containing the alloys, heat developed in the rods and the temperature was increased. MJ47 contains Mn which has higher electrical resistivity [38] than Cr containing in MJ12. Therefore, the electrical power applying to MJ47 is higher than that to MJ12. The carburization temperature of MJ47 is higher than that of MJ12. Jump frequency, diffusion coefficient and quantity of carbon which diffuse into the alloy per unit area in MJ47 is higher than those in MJ12. These reflect the penetration depth, mass increase and density increase of the two alloys.

Table 4.3 The penetration depth, mass increase and density increase for MJ12 and MJ47 by directly applying voltages.

Properties	MJ12	MJ47
Penetration depth ($\times 10^{-6}$ m)	0.72	0.96
Mass increase ($\times 10^{-3}$ kg.m^{-2})	0.72	3.31
Density increase ($\times 10^{3}$ kg.m^{-3})	1.0	3.4

4.4 X-Ray Diffractometer

4.4.1 Nitridation and Carburization by Direct Metal-Gas Reaction

XRD spectra of MJ12 and MJ47 with 1000-1300 K nitridation in10.0 $cm^3.s^{-1}$ NH_3 and carburization in 0.05 $cm^3.s^{-1}$ C_2H_2 are shown in Figure 4.7. Several phases are shown in Table 4.4 and 4.5.

Before nitridation and carburization, TiAl was detected on both MJ12 and MJ47. TiB_2 was detected only on MJ47. After nitridation and carburization, TiAl, Ti_3Al, TiO, TiO_2, Al_2O_3, and C were detected on both MJ12 and MJ47. Only TiB_2 was detected on MJ47. Ti_3Al phase was formed during the nitridation and carburization processes owing to the dissolution of N, C and O in γ-TiAl alloys which increased Ti_3Al volume fraction [26]. Some released Al atoms were oxidized by the impure oxygen to form Al_2O_3. The impure oxygen seems to be from the reactive gases or from the reaction between hydrogen of the reactive gases and the silica containing in the high temperature reaction chamber. Some Ti atoms were also oxidized with the impure oxygen to form TiO and TiO_2. It is not evident that Al, $(TiO_{1.2})_{3.12}$ and C_{60} were formed because their peak are very close to TiAl, TiO and Ti_3Al, respectively. The non-stoichiometric phases of $Ti_{0.992}O_2$, $Ti_{0.936}O_2$, $Ti_{0.928}O_2$, $Ti_{0.924}O_2$ and $Ti_{0.912}O_2$ were possibly detected due to excess O or insufficient of Ti during the nitridation and carburization processes. These non-stoichiometric phases can not clearly analyzed. The excessive carbon atoms can precipitate as solid carbon phases on the alloy surfaces .

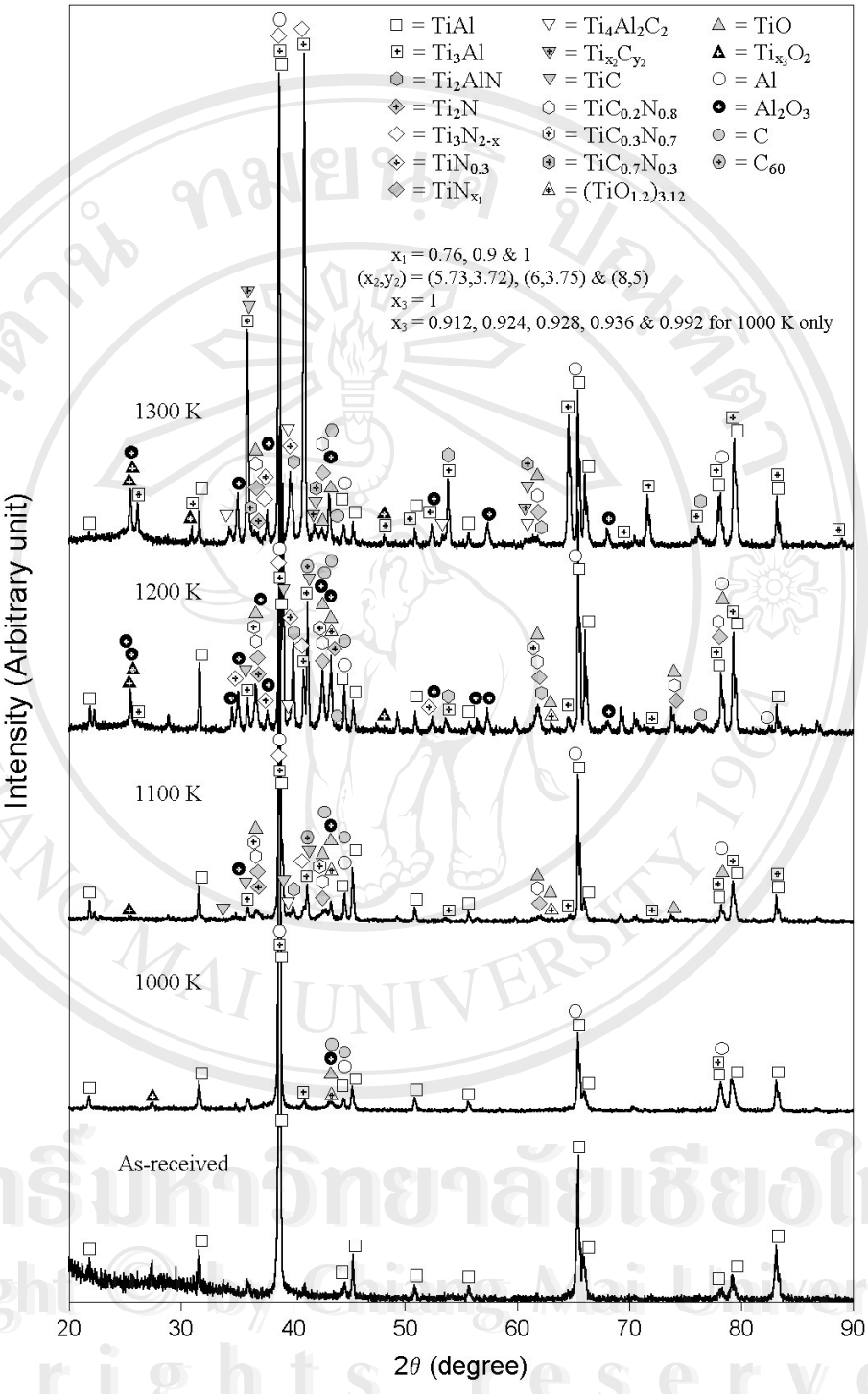

(a)

(Figure is continued to next page.)

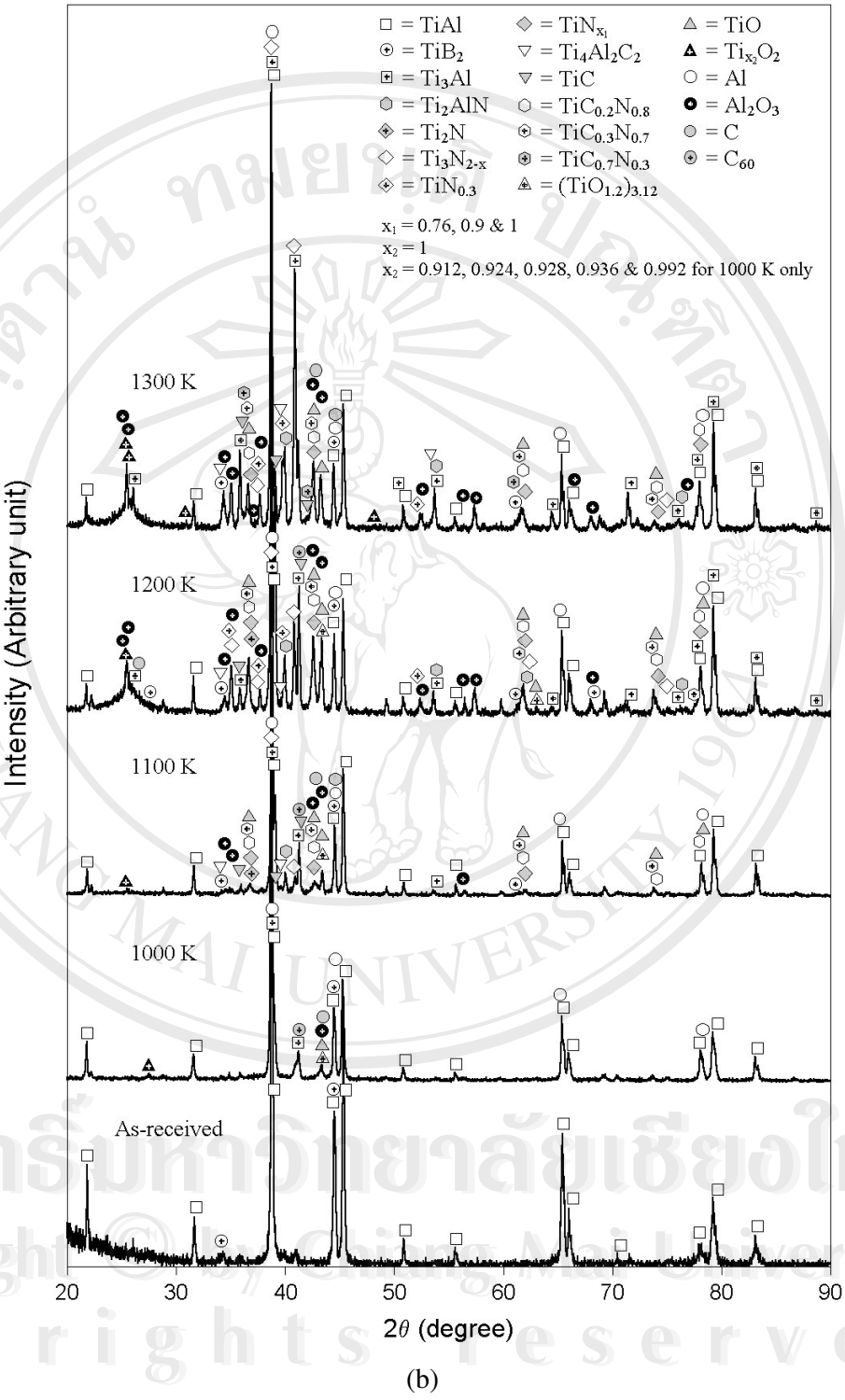

(b)

Figure 4.7 XRD spectra of (a) MJ12 and (b) MJ47 with 1000–1300 K nitridation in 10.0 $cm^3.s^{-1}$ NH_3 and carburization in 0.05 $cm^3.s^{-1}$ C_2H_2.

Table 4.4 Collection of the phases formed on MJ12 and MJ47 during nitridation and carburization.

T (K)	MJ12	MJ47
As-received	TiAl	TiAl, TiB_2
1000	TiAl	TiAl, TiO_2,
1100	TiAl, Ti_3Al, Ti_2AlN, TiO_2	TiAl, $Ti_4Al_2C_2$, TiO_2, Al_2O_3,
1200	TiAl, Ti_3Al, Ti_2AlN, TiO_2, Al, Al_2O_3	TiAl, Ti_3Al, Al_2O_3,
1300	TiAl, Ti_3Al, $Ti_4Al_2C_2$, TiO_2, Al_2O_3	TiAl, Ti_3Al, TiO_2, Al_2O_3,

Table 4.5 Collection of the phases possibly formed on MJ12 and MJ47 during nitridation and carburization.

T (K)	MJ12	MJ47
As-received	-	-
1000	Ti_3Al, TiO_2, $(TiO_{1.2})_{3.12}$, TiO, $Ti_{0.992}O_2$, $Ti_{0.936}O_2$, $Ti_{0.928}O_2$, $Ti_{0.924}O_2$, $Ti_{0.912}O_2$, Al, Al_2O_3, C	TiB_2, Ti_3Al, Al, $(TiO_{1.2})_{3.12}$, TiO, $Ti_{0.992}O_2$, $Ti_{0.936}O_2$, $Ti_{0.928}O_2$, $Ti_{0.924}O_2$, $Ti_{0.912}O_2$, Al_2O_3, C, C_{60}
1100	Ti_2N, Ti_3N_{2-x}, $TiN_{0.76}$, $TiN_{0.9}$, TiN, $Ti_4Al_2C_2$,TiC, $TiC_{0.2}N_{0.8}$, $TiC_{0.3}N_{0.7}$, $(TiO_{1.2})_{3.12}$, TiO, Al, Al_2O_3, C, C_{60}	TiB_2, Ti_3Al, Ti_2AlN, Ti_2N, Ti_3N_{2-x}, $TiN_{0.76}$, $TiN_{0.9}$, TiN, TiC, $TiC_{0.2}N_{0.8}$, $TiC_{0.3}N_{0.7}$, $(TiO_{1.2})_{3.12}$, TiO, Al, C, C_{60}
1200	Ti_2N, Ti_3N_{2-x}, $TiN_{0.3}$, $TiN_{0.76}$, $TiN_{0.9}$, TiN, $Ti_4Al_2C_2$, TiC, $TiC_{0.2}N_{0.8}$, $TiC_{0.3}N_{0.7}$, $(TiO_{1.2})_{3.12}$, TiO, TiO_2, C, C_{60}	TiB_2, Ti_2AlN, Ti_2N, Ti_3N_{2-x}, $TiN_{0.3}$, $TiN_{0.76}$, $TiN_{0.9}$, TiN, $Ti_4Al_2C_2$, TiC, $TiC_{0.2}N_{0.8}$, $TiC_{0.3}N_{0.7}$, $(TiO_{1.2})_{3.12}$, TiO, TiO_2, Al, C, C_{60}
1300	Ti_2AlN, Ti_2N, Ti_3N_{2-x}, $TiN_{0.3}$, $TiN_{0.76}$, $TiN_{0.9}$, TiN, $Ti_{5.73}C_{3.72}$, $Ti_6C_{3.75}$, Ti_8C_5, TiC, $TiC_{0.2}N_{0.8}$, $TiC_{0.7}N_{0.3}$, TiO, Al, C	TiB_2, Ti_2AlN, Ti_2N, Ti_3N_{2-x}, $TiN_{0.3}$, $TiN_{0.76}$, $TiN_{0.9}$, TiN, $Ti_4Al_2C_2$, TiC, $TiC_{0.2}N_{0.8}$, $TiC_{0.3}N_{0.7}$, $TiC_{0.7}N_{0.3}$, TiO, Al, C

During the nitridation and carburization processes, some NH_3 and C_2H_2 decomposed into N, H and C. Some H, N and C atoms adsorbed on the surface of the alloys and dissolved into the matrices. When N and C concentrations exceeded solubility limit of the alloys, they reacted with Ti and Al, and several phases of nitrides, carbides and carbonitrides formed. Hydrides can from as well but the reduction of H by the impure O could lead to the low hydride concentration which is too low to be detected. At 1000 K nitridation and carburization, no nitrides and carbides were detected. Their concentrations could be too low to be detected or the temperature was too low to form nitrided and carbided phases. The detection of Ti_3Al reflects the dissolution of N, C and O in alloy matrices. The concentration is not enough to form nitride or carbide. At 1100 – 1300 K nitridation and carburization, the additional phases of different nitrides, carbonitrides and carbides seem to be detected. $TiN_{0.76}$, $TiN_{0.9}$, TiN, $TiC_{0.2}N_{0.8}$, $TiC_{0.3}N_{0.7}$, TiC and $TiC_{0.7}N_{0.3}$ can not be determined clearly.

4.4.2 Nitridation by Direct Metal-Gas Reaction

XRD spectra of MJ12 and MJ47 with 1000-1300 K nitridation are shown in Figure 4.8. Several phases formed and possibly formed on both alloys at different temperatures and were collected in Table 4.6 and 4.7. At 1000 K, no nitride was detected. At 1100 K and above, TiN were detected. Its non-stoichiometric phases are able to form as well. The XRD spectra reveal that the concentration of nitrides were increased with the increase of temperature.

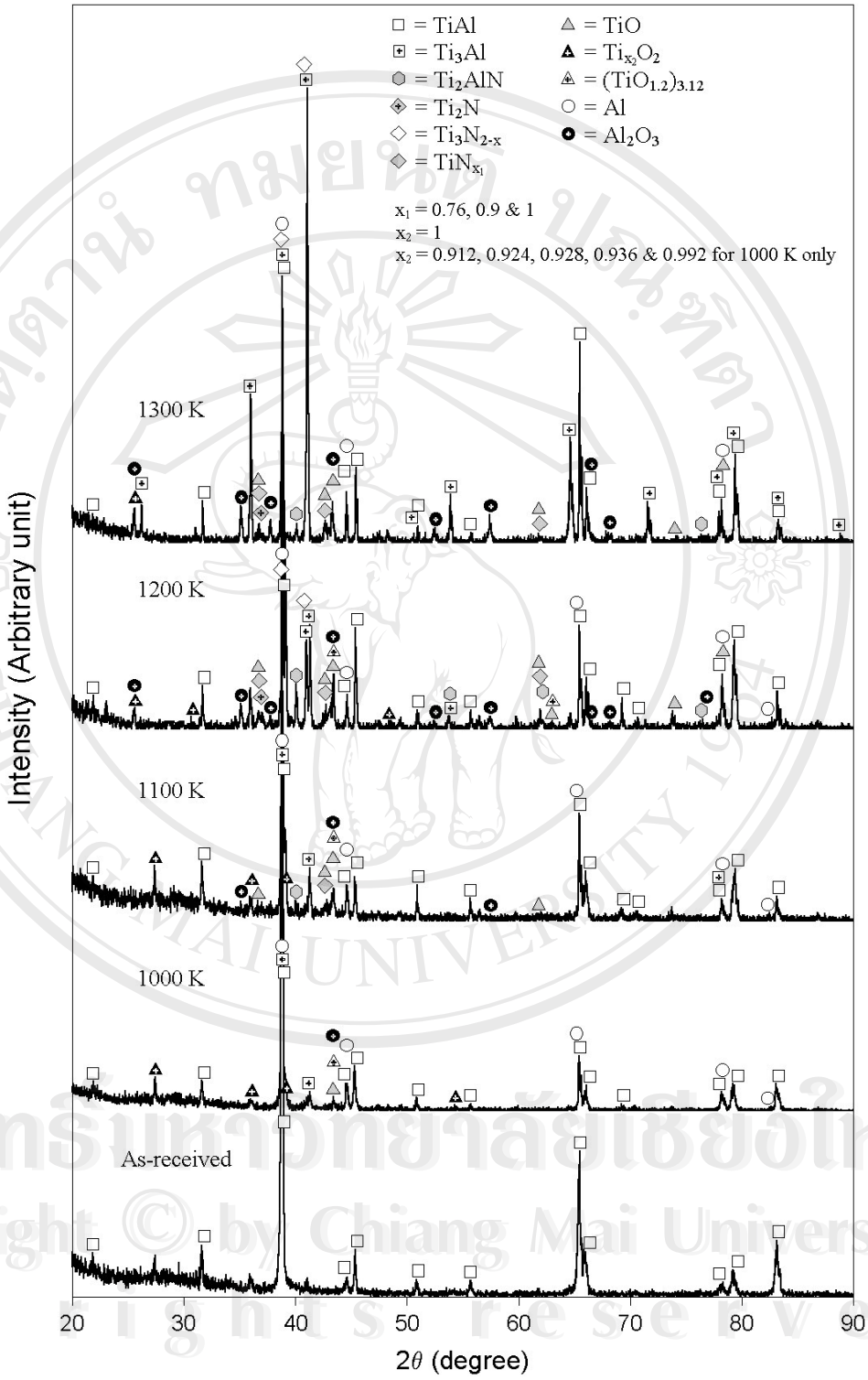

(a)

(Figure is continued to next page.)

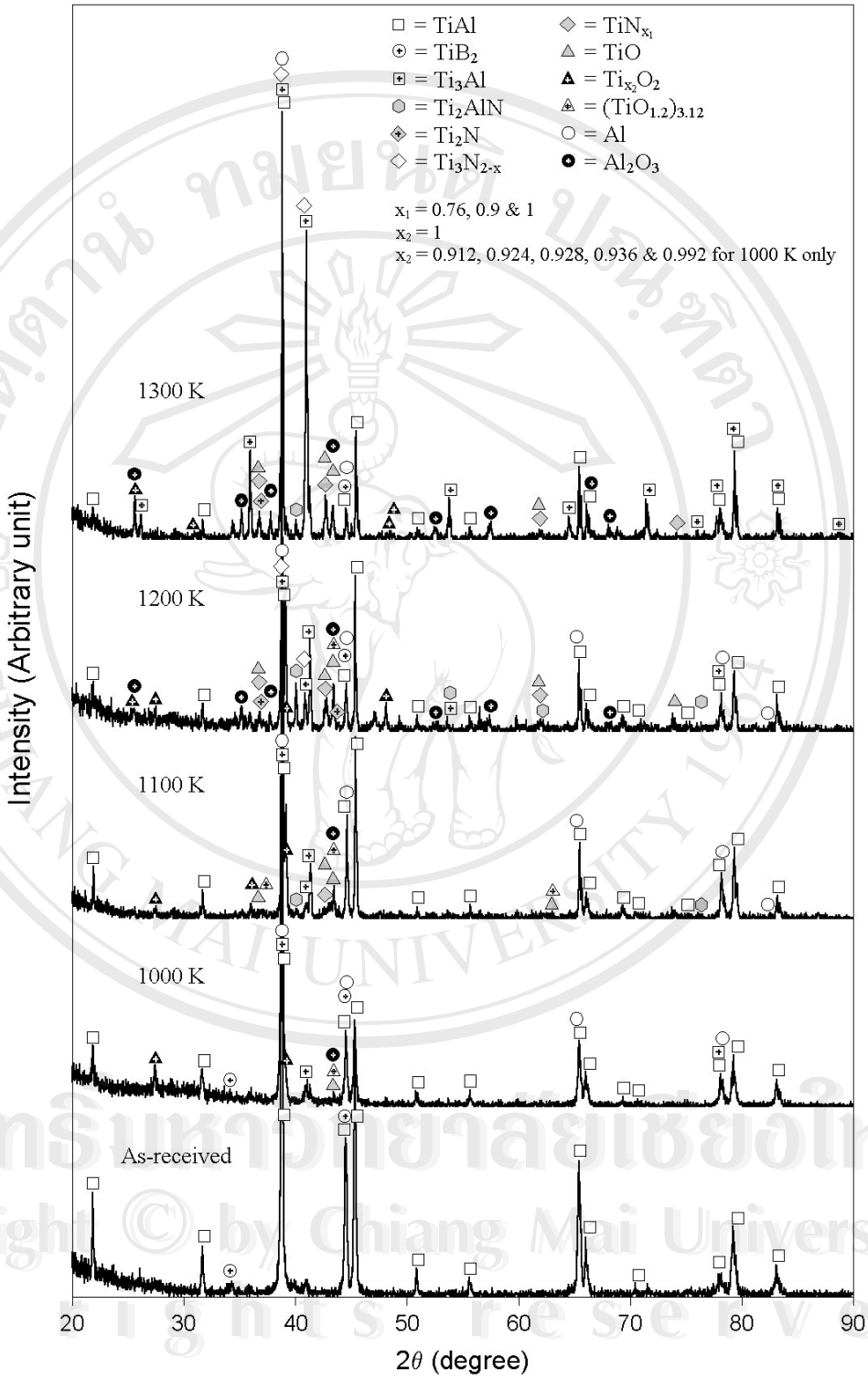

(b)

Figure 4.8 XRD spectra of (a) MJ12 and (b) MJ47 with 1000–1300 K nitridation.

Table 4.6 Collection of the phases formed on MJ12 and MJ47 during nitridation.

T (K)	MJ12	MJ47
As-received	TiAl	TiAl, TiB_2
1000	TiAl, Ti_3Al, Al	TiAl, TiB_2, Ti_3Al
1100	TiAl, Ti_3Al, Ti_2AlN, TiO, Al, Al_2O_3	TiAl, Ti_3Al, Ti_2AlN, Al
1200	TiAl, Ti_3Al, Ti_2AlN, TiO, TiO_2, Al, Al_2O_3	TiAl, Ti_3Al, Ti_2AlN, TiO, Al, Al_2O_3,
1300	TiAl, Ti_3Al, Ti_2AlN, TiO, Al_2O_3	TiAl, Ti_3Al, Ti_2AlN, TiO_2, Al_2O_3

Table 4.7 Collection of the phases possibly formed on MJ12 and MJ47 during nitridation.

T (K)	MJ12	MJ47
As-received	-	-
1000	TiO, TiO_2, $Ti_{0.992}O_2$, $Ti_{0.936}O_2$, $Ti_{0.928}O_2$, $Ti_{0.924}O_2$, $Ti_{0.912}O_2$, $(TiO_{1.2})_{3.12}$, Al_2O_3	TiO, TiO_2, $Ti_{0.992}O_2$, $Ti_{0.936}O_2$, $Ti_{0.928}O_2$, $Ti_{0.924}O_2$, $Ti_{0.912}O_2$, $(TiO_{1.2})_{3.12}$, Al, Al_2O_3
1100	$TiN_{0.76}$, $TiN_{0.9}$, TiN, TiO_2, $Ti_{0.992}O_2$, $Ti_{0.936}O_2$, $Ti_{0.928}O_2$, $Ti_{0.924}O_2$, $Ti_{0.912}O_2$, $(TiO_{1.2})_{3.12}$	TiB_2, $TiN_{0.76}$, $TiN_{0.9}$, TiN, TiO, TiO_2, $Ti_{0.992}O_2$, $Ti_{0.936}O_2$, $Ti_{0.928}O_2$, $Ti_{0.924}O_2$, $Ti_{0.912}O_2$, $(TiO_{1.2})_{3.12}$, Al_2O_3
1200	Ti_2N, Ti_3N_{2-x}, $TiN_{0.76}$, $TiN_{0.9}$, TiN, $(TiO_{1.2})_{3.12}$	TiB_2, Ti_2N, Ti_3N_{2-x}, $TiN_{0.76}$, $TiN_{0.9}$, TiN, TiO_2, $(TiO_{1.2})_{3.12}$
1300	Ti_2N, Ti_3N_{2-x}, $TiN_{0.76}$, $TiN_{0.9}$, TiN, TiO_2, Al	TiB_2, Ti_2N, Ti_3N_{2-x}, $TiN_{0.76}$, $TiN_{0.9}$, TiN, TiO, Al

4.4.3 Carburization by Directly Applying Voltages

Figure 4.9 shows the XRD spectra of MJ12 and MJ47. Before carburization, TiAl was detected on both alloys. TiB_2 was detected on only MJ47. After carburization of MJ12, new phases of TiC, TiO_2 and C formed and Ti_3Al, TiO, $Ti_{0.992}O_2$, $Ti_{0.936}O_2$, $Ti_{0.928}O_2$, $Ti_{0.924}O_2$, $Ti_{0.912}O_2$ $(TiO_{1.2})_{3.12}$, Al, Al_2O_3 and C_{60} possibly formed. But for MJ47, new phases of Ti_3Al, TiO, TiO_2, Al_2O_3 and C formed and TiC, $Ti_{0.992}O_2$, $Ti_{0.936}O_2$, $Ti_{0.928}O_2$, $Ti_{0.924}O_2$, $Ti_{0.912}O_2$ $(TiO_{1.2})_{3.12}$, Al, and C_{60} possibly formed. This shows that TiC can be deposited on the γ-TiAl alloys by directly applying voltages. The detection of Al_2O_3, TiO, TiO_2 and their non-stochiometric compounds seems to be the reaction of the metals with the impure oxygen containing in Ar.

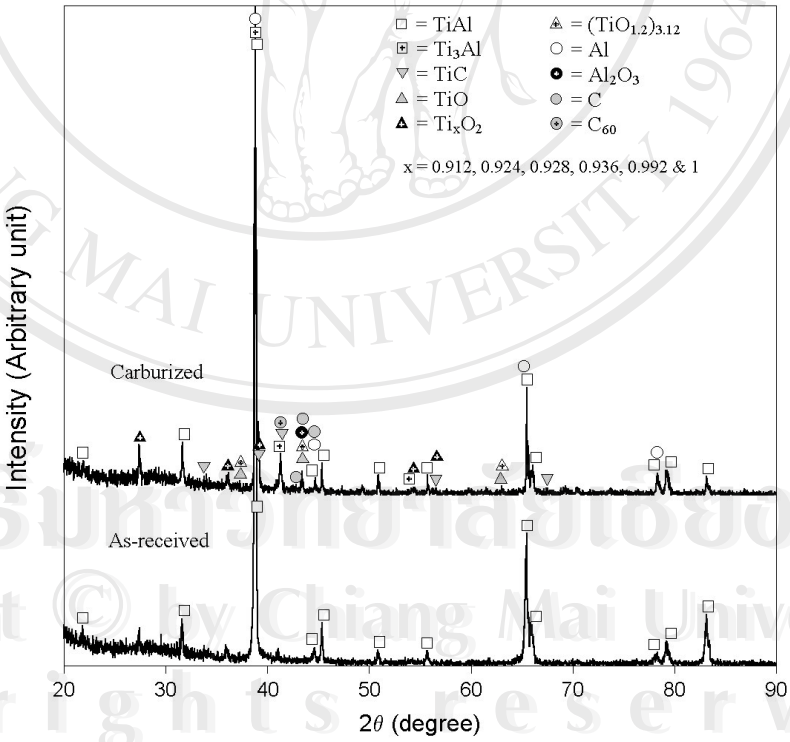

(a)

(Figure is continued to next page.)

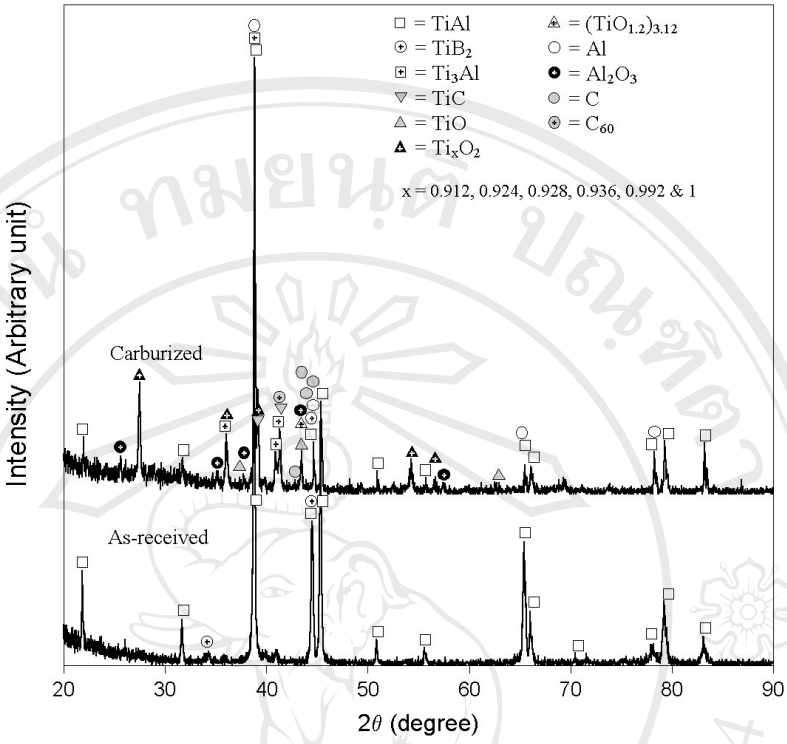

(b)

Figure 4.9 XRD spectra of (a) MJ12 and (b) MJ47 before and after carburization.

4.5 Energy Dispersive X-ray

4.5.1 Nitridation and Carburization by Direct Metal-Gas Reaction

EDX spectra of the alloys without and with 1000-1300 K nitridation in 10 $cm^3.s^{-1}$ NH_3 and carburization in 0.01, 0.03 and 0.05 $cm^3.s^{-1}$ C_2H_2 are shown in Figure 4.10 to Figure 4.12. Before nitridation and carburization, Ti, Al, Nb and Cr were detected on MJ12 and Ti, Al, Nb, and Mn were detected on MJ47. No B was detected on MJ47 due to its low atomic mass and concentration. After the nitridation and carburization, N, C and O atoms were also detected on both alloys. This shows that the scale contains the dissolved nitrogen, carbon and oxygen. The results are in agreement with the XRD detection. At high temperature nitridation and carburization and at high C_2H_2 flow rate, the intensity of Nb, Cr and Mn was rather low. It is suggest that during the nitridation and carburization processes at high temperature and

at high C_2H_2 flow rate, more Ti atoms diffused outward to metal-scale interface and more Nb, Cr and Mn atoms diffuse inward to fill the titanium vacancies. At high temperature nitridation and carburization and at high C_2H_2 flow rate, the intensity of C is rather high. This shows that there is high quantity of solid carbon deposited on the surface of the alloys.

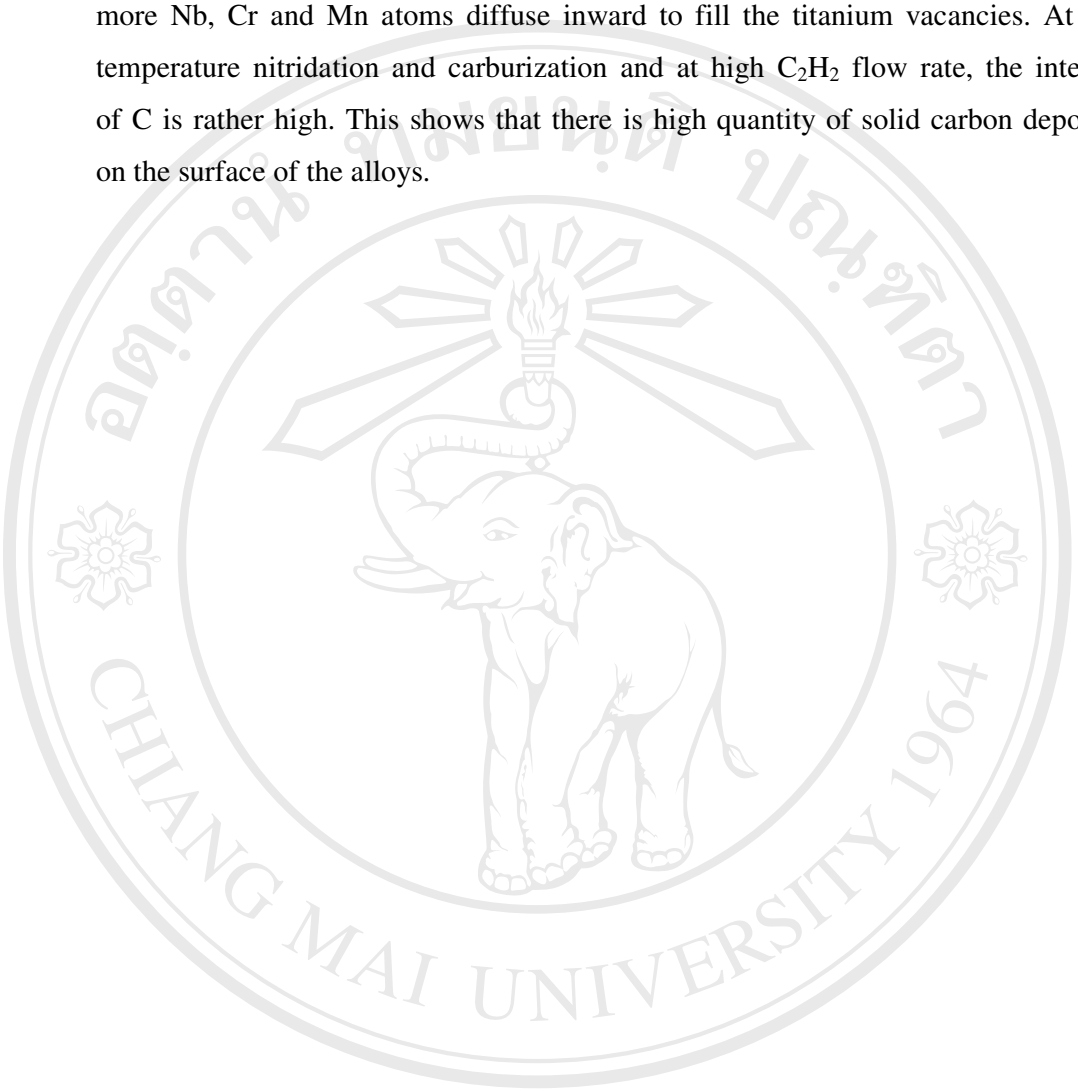

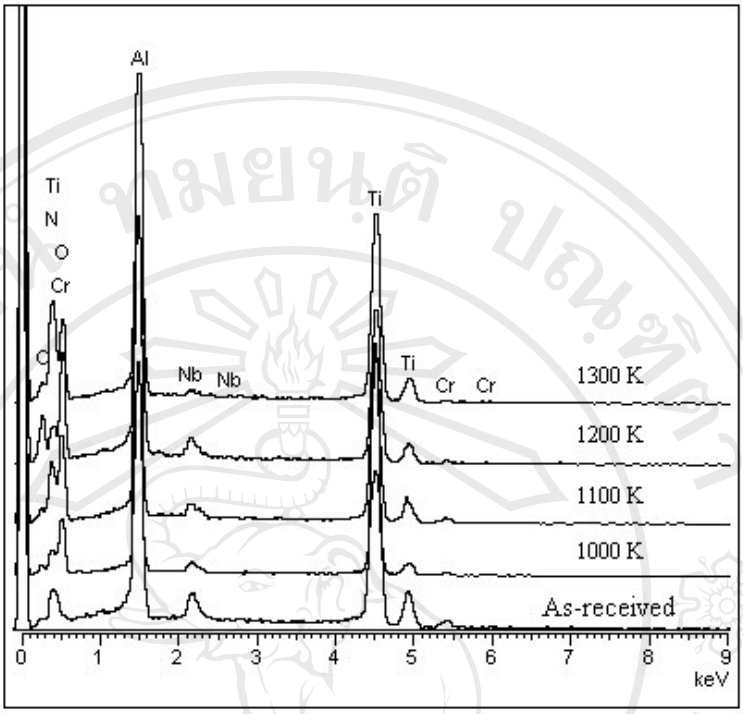

(a)

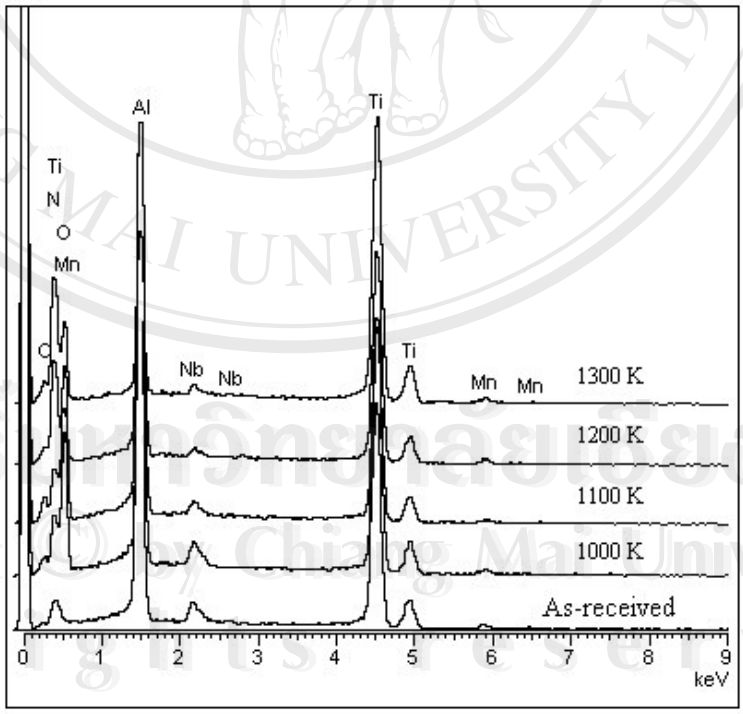

(b)

Figure 4.10 EDX spectra of (a) MJ12 and (b) MJ47 without and with 1000-1300 K nitridation and carburization in 10 $cm^3.s^{-1}$ NH_3 and 0.01 $cm^3.s^{-1}$ C_2H_2.

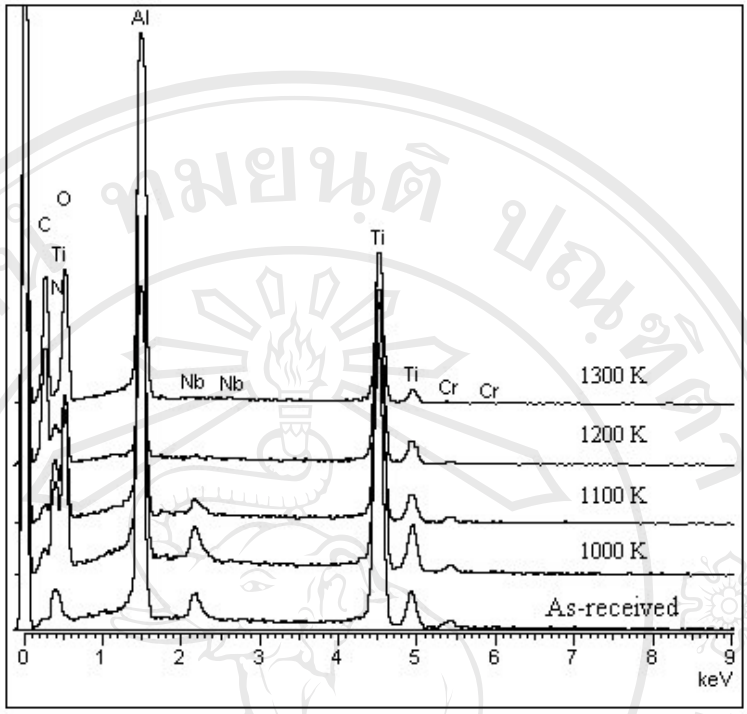

(a)

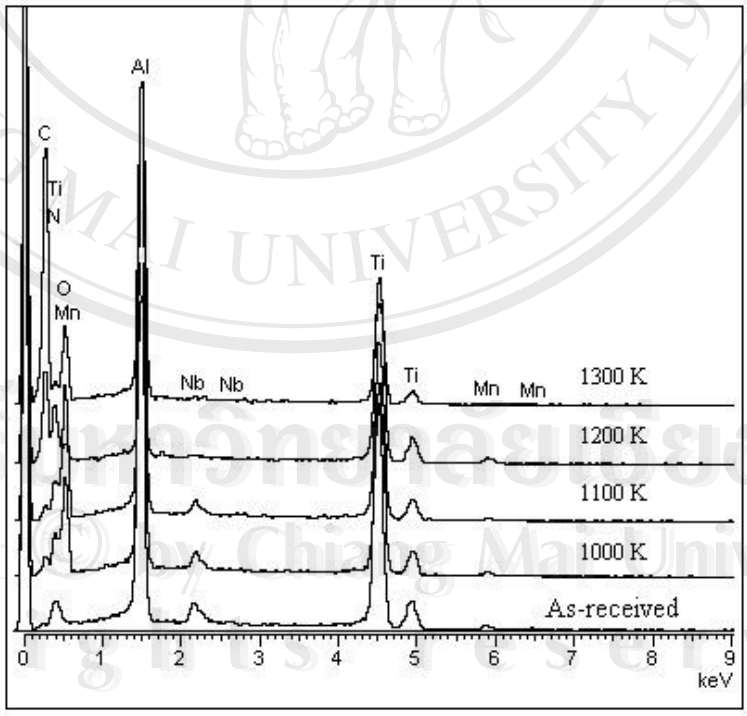

(b)

Figure 4.11 EDX spectra of (a) MJ12 and (b) MJ47 without and with 1000-1300 K nitridation and carburization in 10 $cm^3.s^{-1}$ NH_3 and 0.03 $cm^3.s^{-1}$ C_2H_2.

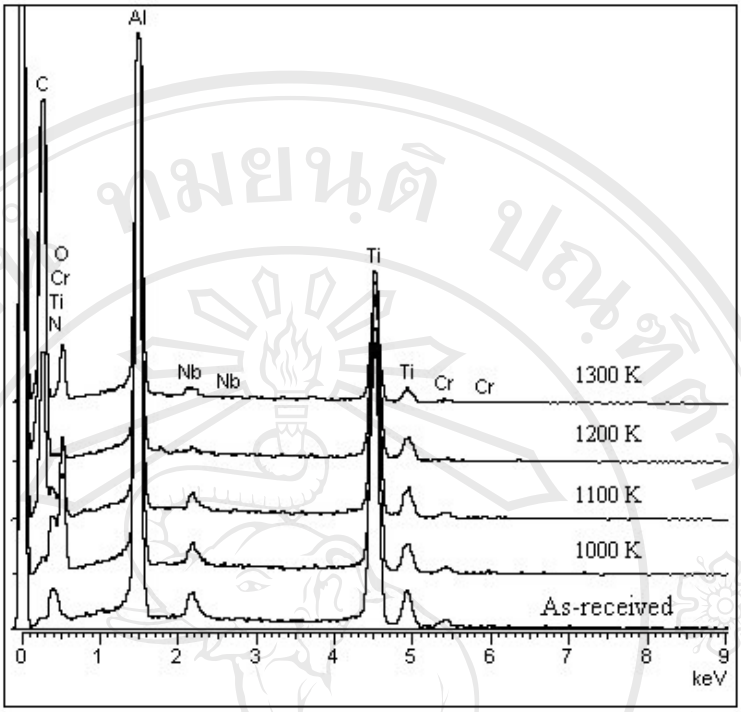

(a)

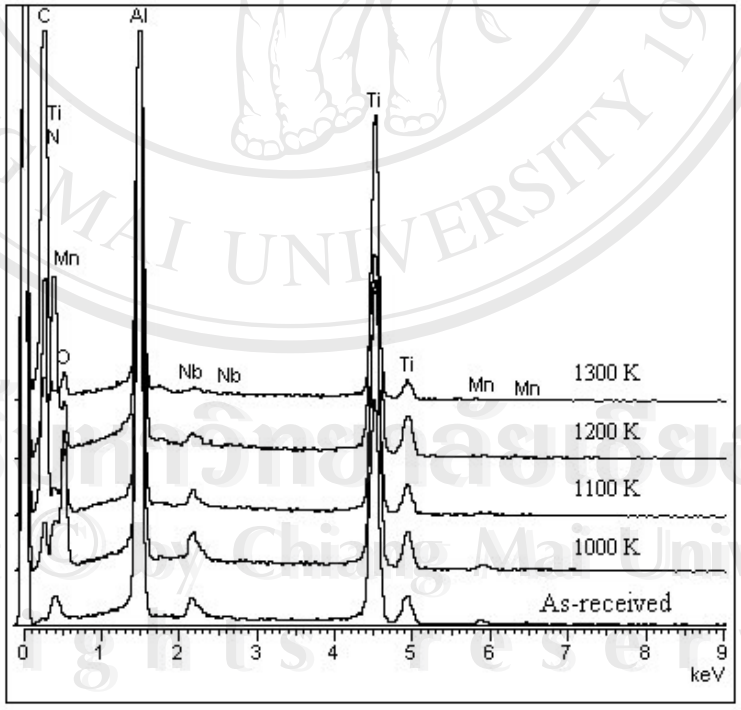

(b)

Figure 4.12 EDX spectra of (a) MJ12 and (b) MJ47 without and with 1000-1300 K nitridation and carburization in 10 $cm^3.s^{-1}$ NH_3 and 0.05 $cm^3.s^{-1}$ C_2H_2.

4.5.2 Nitridation by Direct Metal-Gas Reaction

The EDX spectra of the alloys without and with 1000-1300 K nitridation are shown in Figure 4.13. Before nitridation, Ti, Al and Nb were detected on both alloys. Cr and Mn were detected on MJ12 and MJ47, respectively. There was no detection of B. After nitridation, N and O were detected on both alloys. The spectra reveal the dissolution of nitrogen in the alloy matrices during nitridation process. The EDX and XRD analyses show that the results are in consistency.

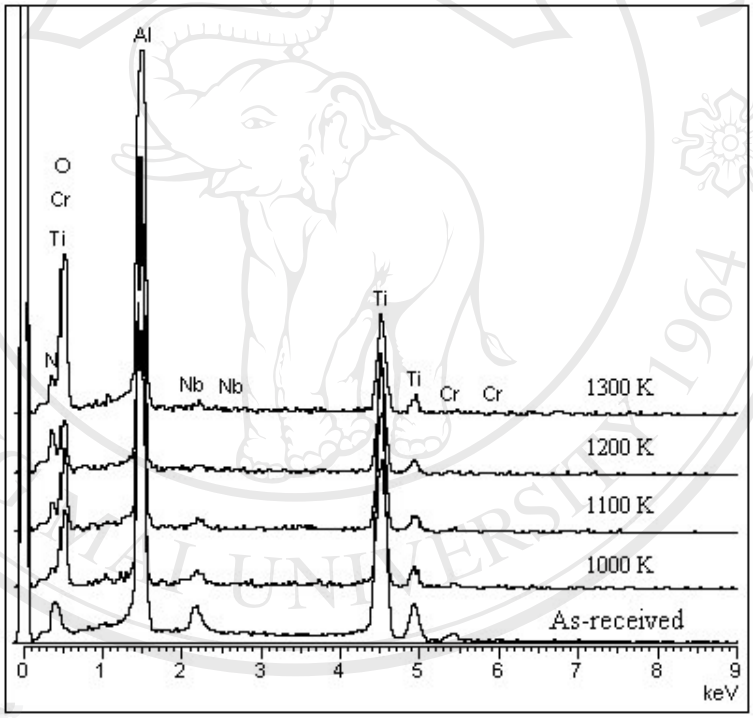

(a)

(Figure is continued to next page.)

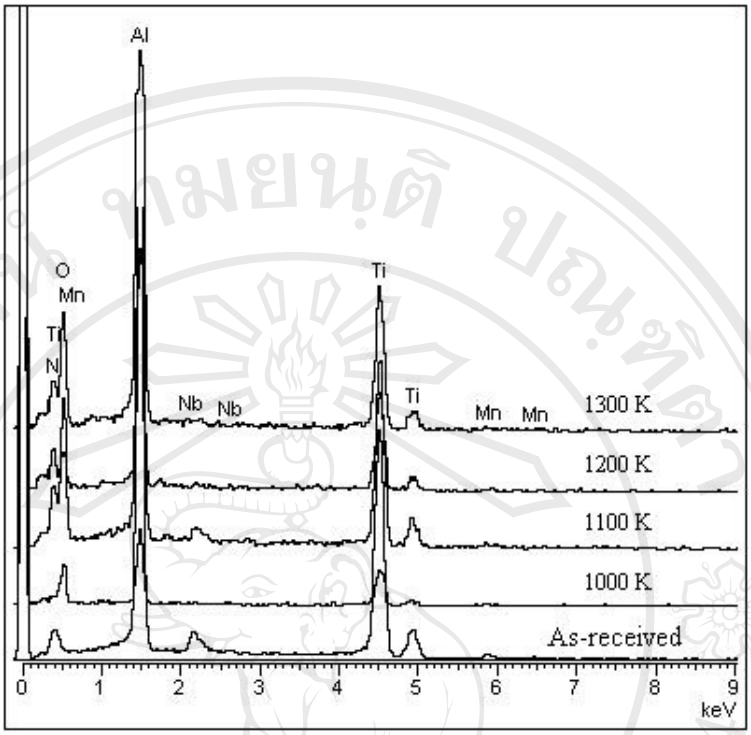

(b)

Figure 4.13 EDX spectra of (a) MJ12 and (b) MJ47 without and with 1000-1300 K nitridation.

4.5.3 Carburization by Directly Applying Voltages

Figure 4.14 shows EDX spectra of the alloys before and after carburization. Before carburization, Ti, Al, Nb and Cr were detected on MJ12. Ti, Al, Nb, and Mn were detected on MJ47. After carburization, C and O were detected on both alloys. This shows that the scale contains carbon and oxygen. The results corresponds to the XRD analysis.

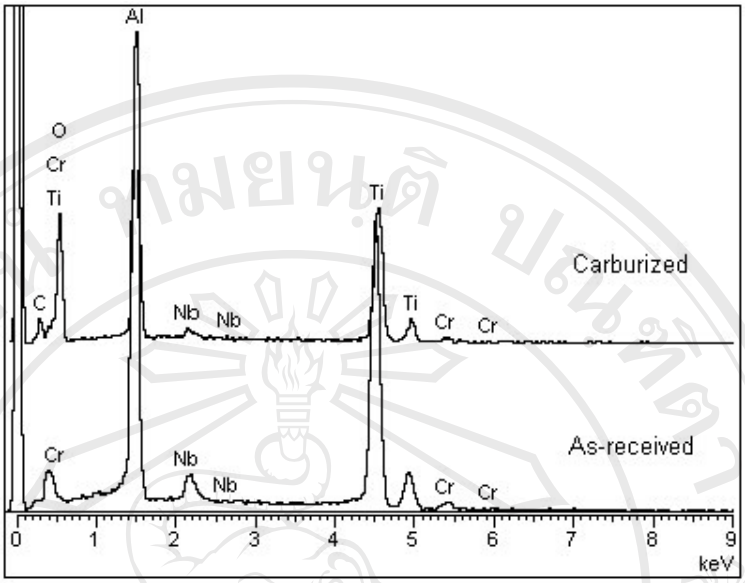

(a)

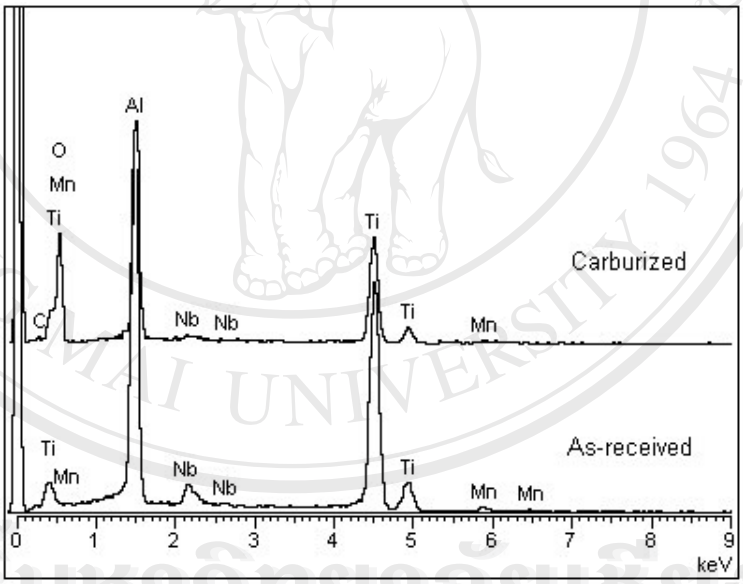

(b)

Figure 4.14 EDX spectra of (a) MJ12 and (b) MJ47 before and after carburization.

4.6 Scanning Electron Microscopy

4.6.1 Nitridation and Carburization by Direct Metal-Gas Reaction

SEM micrographs of the alloys without and with 1000-1300 K nitridation and carburization are given in Figure 4.15 to Figure 4.19. The micrographs reveal the new phases deposited on the alloys after nitridation and carburization. At low temperature nitridation and carburization, needle-liked, irregular shape and round particles formed on the surface of the alloys. Only irregular shape and round particles formed at high temperature nitridation and carburization.

The observation demonstrated that after nitridation and carburization in 0.01 $cm^3.s^{-1}$ C_2H_2 flow rate, the particles are sharp edge. In case of nitridation in 10 $cm^3.s^{-1}$ NH_3 and carburization in 0.05 $cm^3.s^{-1}$ C_2H_2, the particles are round shape. This shows that carbon potential influence the surface morphology of the alloys.

(a)

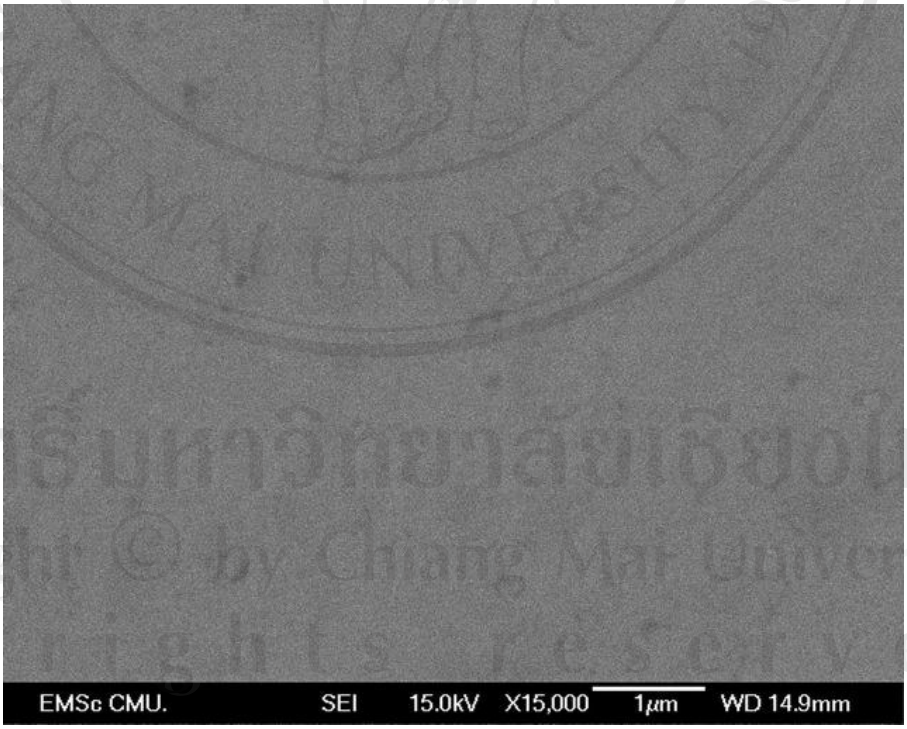

(b)

Figure 4.15 SEM micrographs of the as-received (a) MJ12 and (b) MJ47.

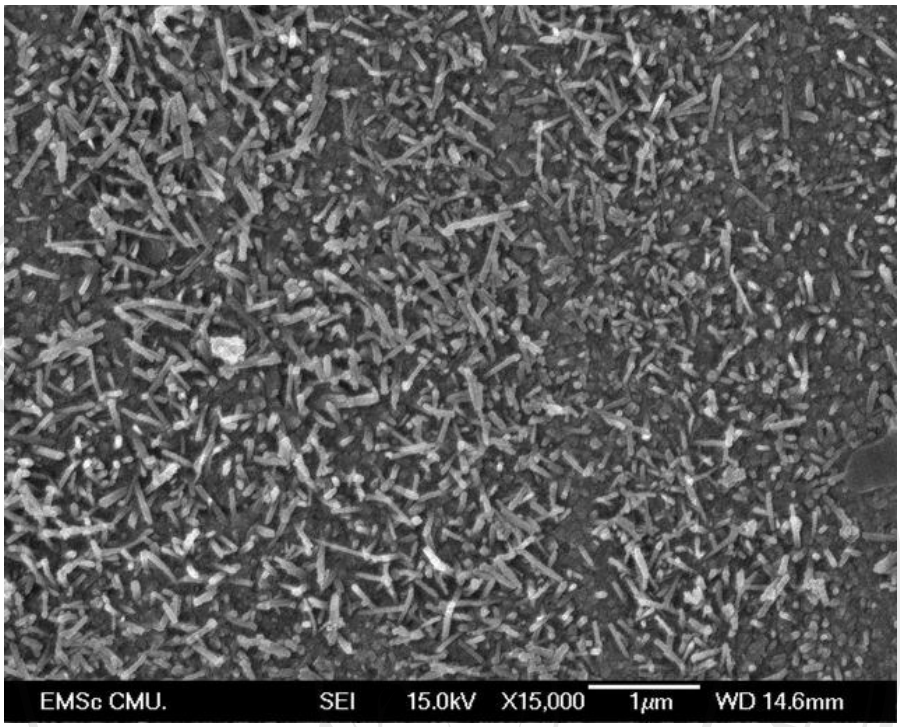

(a)

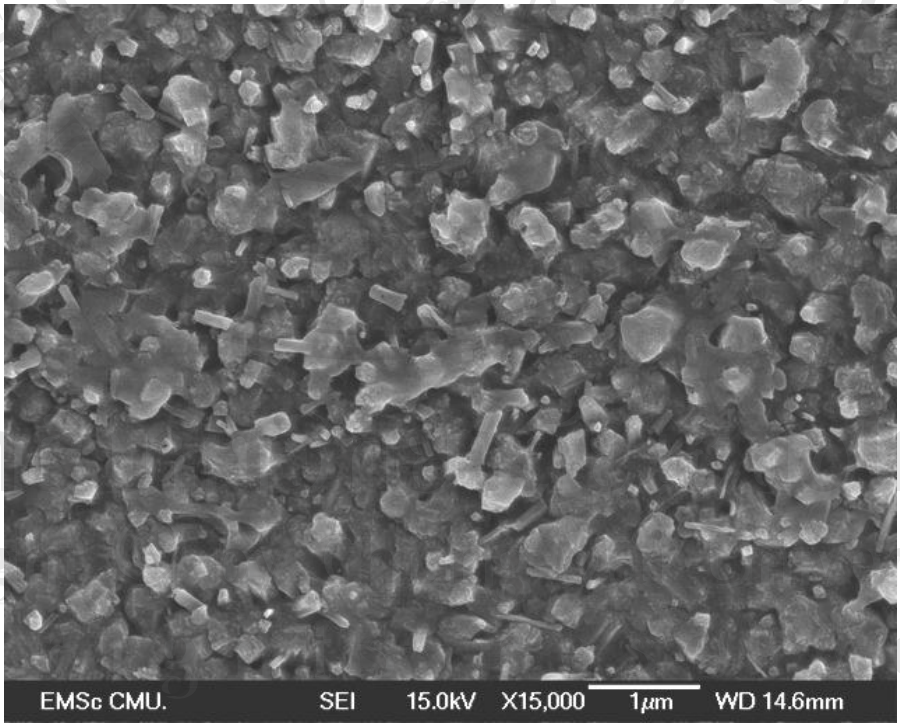

(b)

(Figure is continued to next page.)

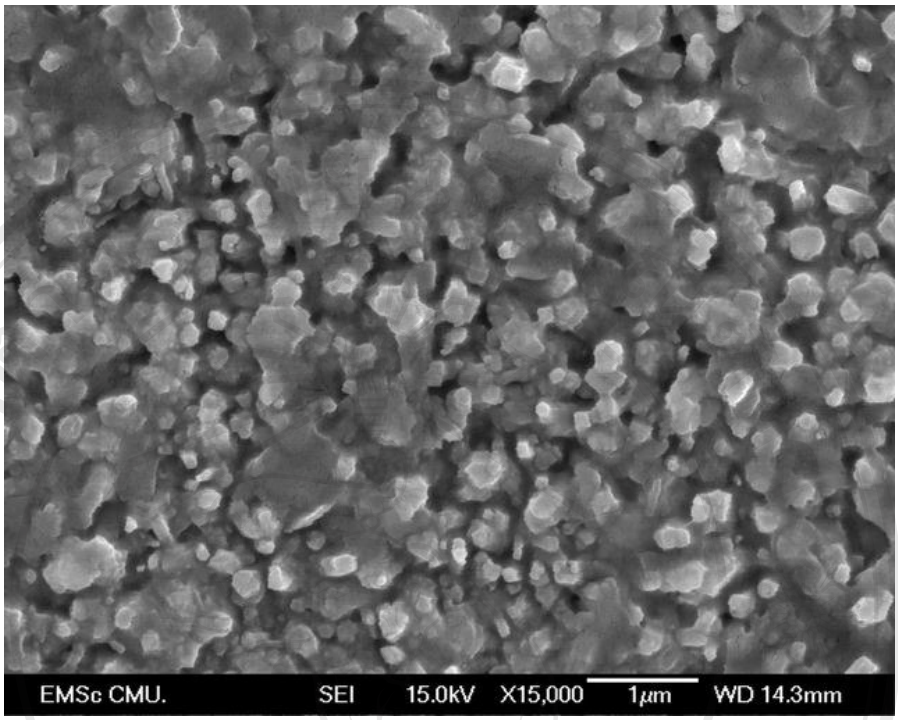

(c)

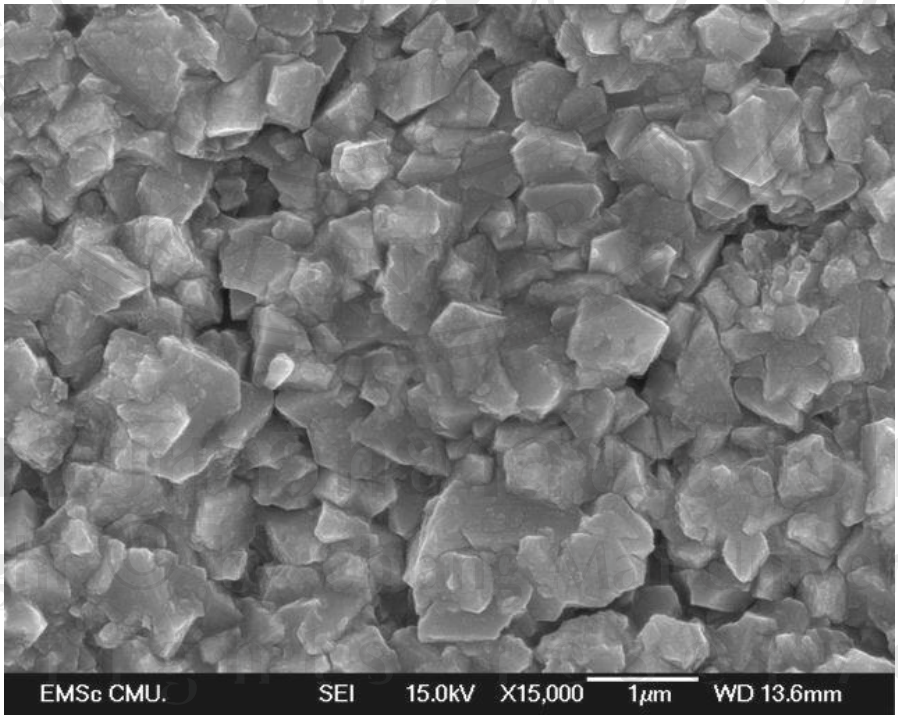

(d)

Figure 4.16 SEM micrographs of MJ12 with (a) 1000 K (b) 1100 K (c) 1200 K and (d) 1300 K nitridation in 10 $cm^3.s^{-1}$ NH_3 and carburization in 0.01 $cm^3.s^{-1}$ C_2H_2.

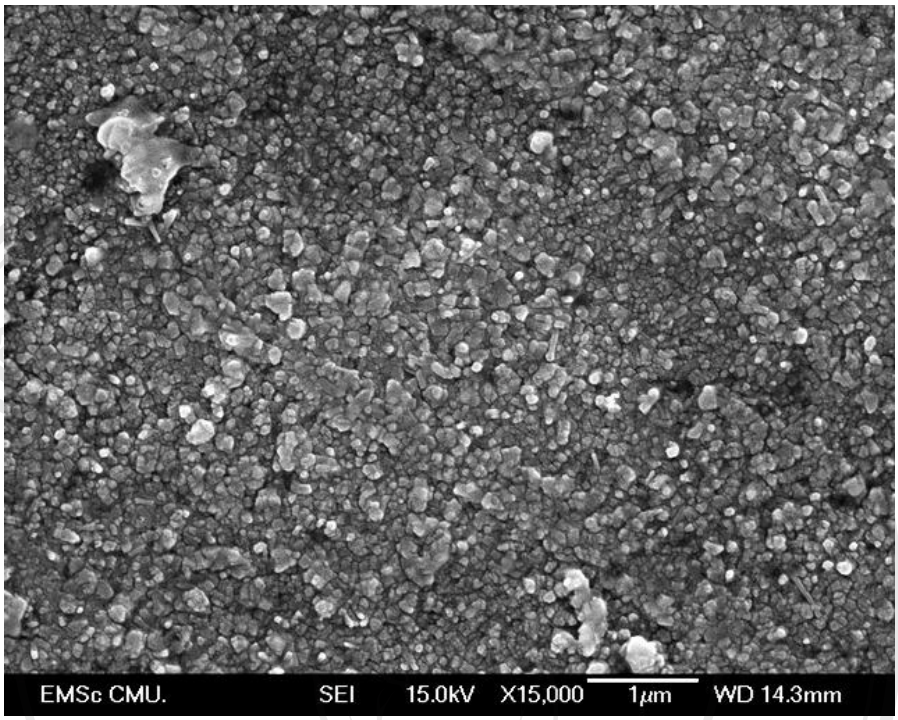

(a)

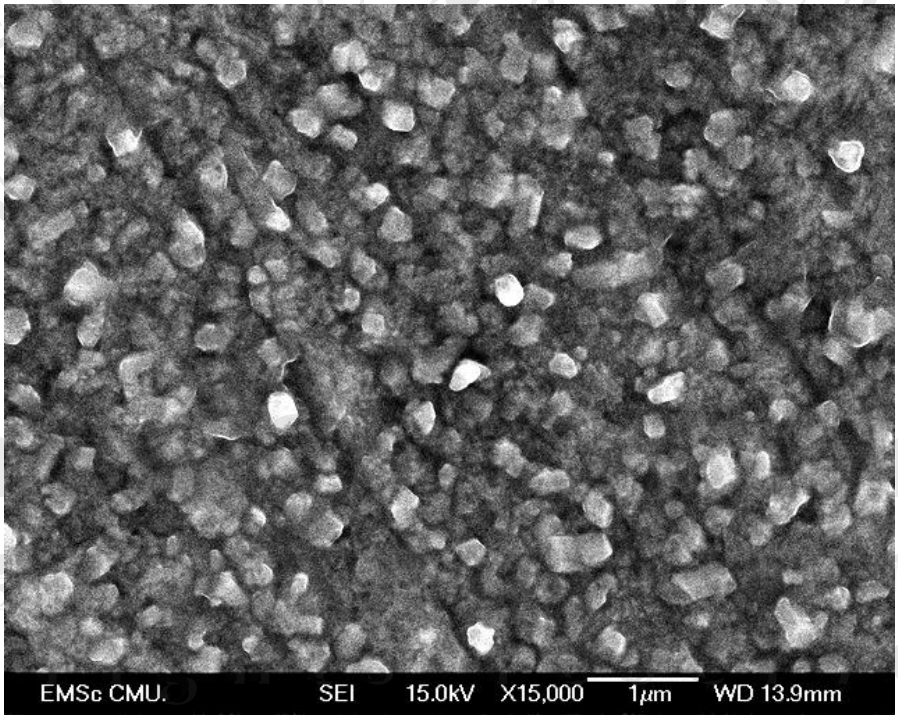

(b)

(Figure is continued to next page.)

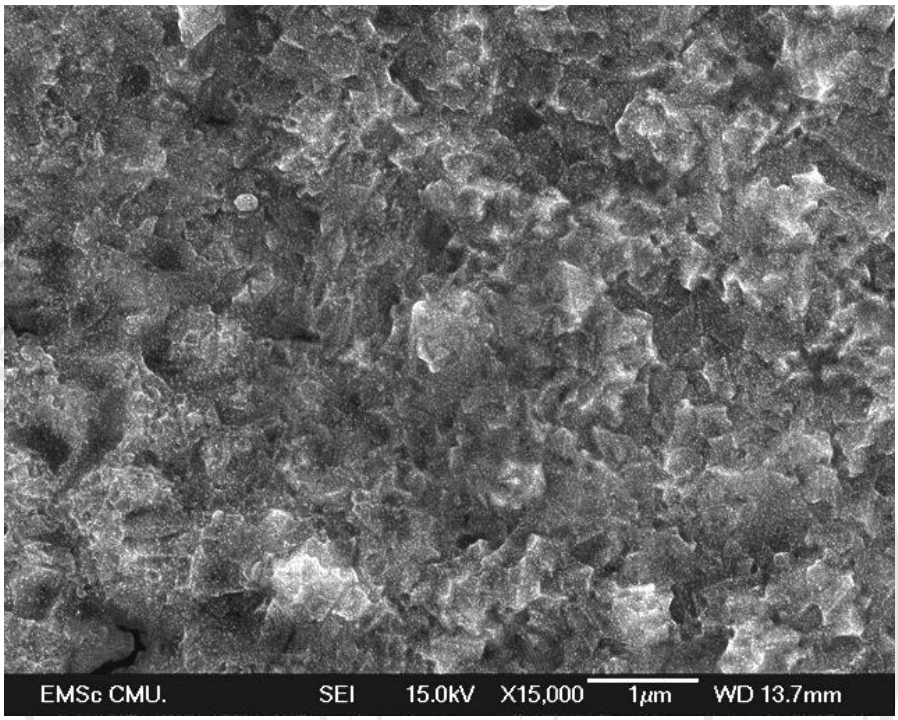

(c)

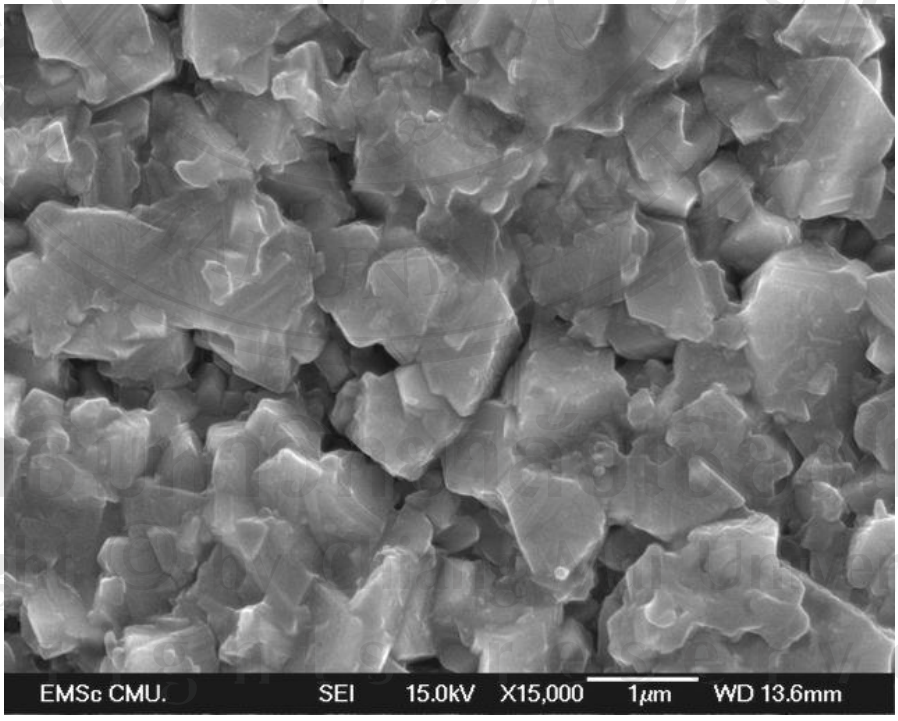

(d)

Figure 4.17 SEM micrographs of MJ47 with (a) 1000 K (b) 1100 K (c) 1200 K and (d) 1300 K nitridation in 10 $cm^3.s^{-1}$ NH_3 and carburization in 0.01 $cm^3.s^{-1}$ C_2H_2.

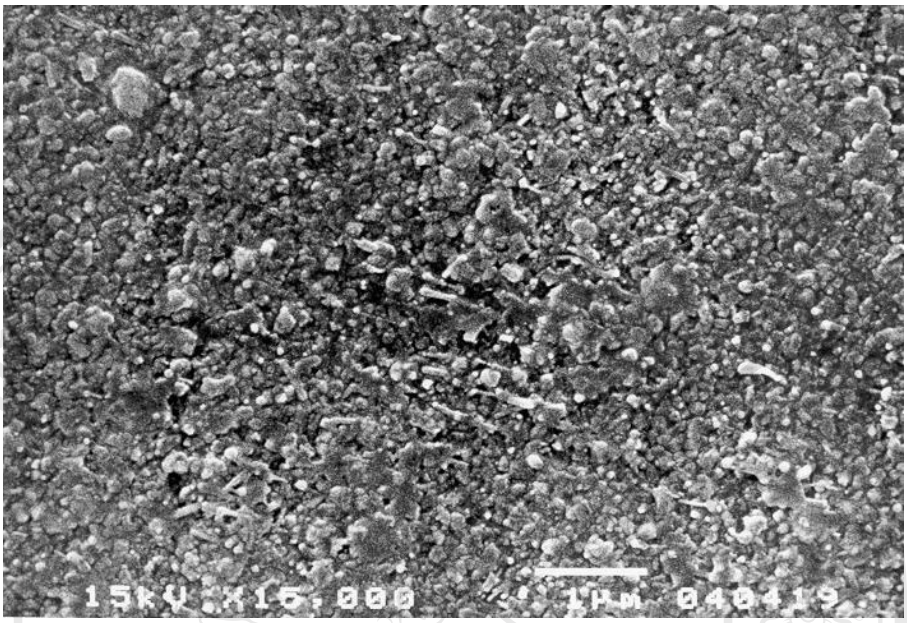

(a)

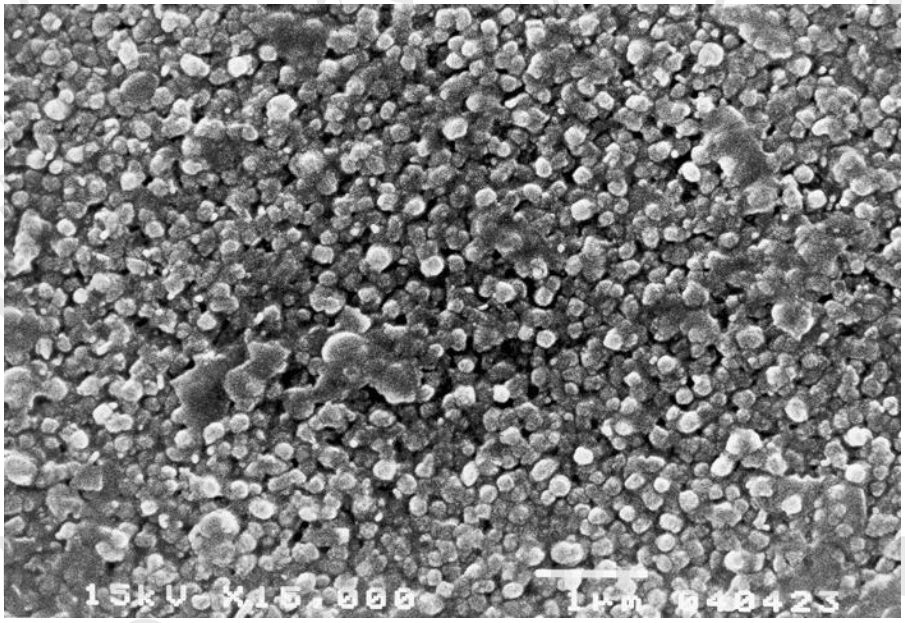

(b)

(Figure is continued to next page.)

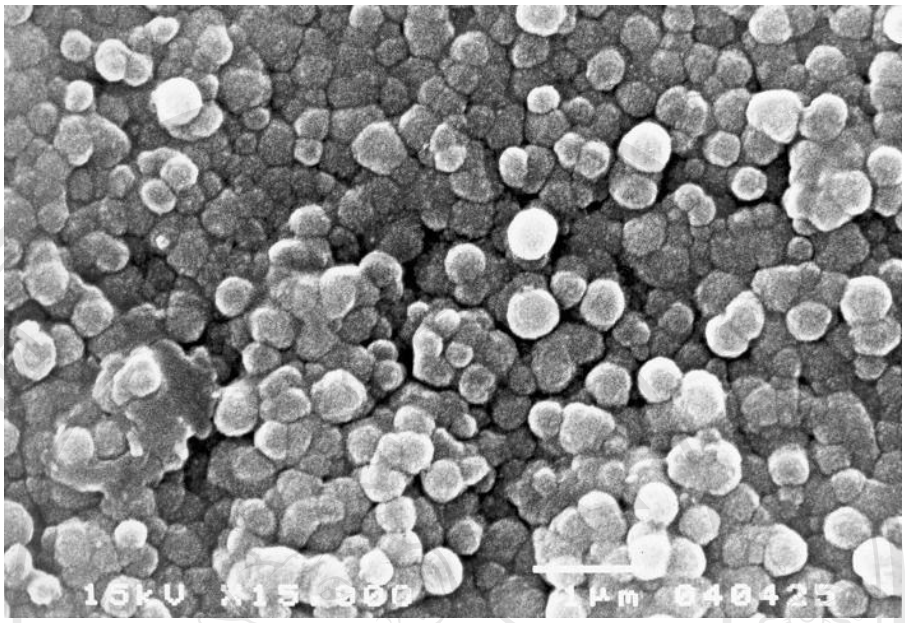

(c)

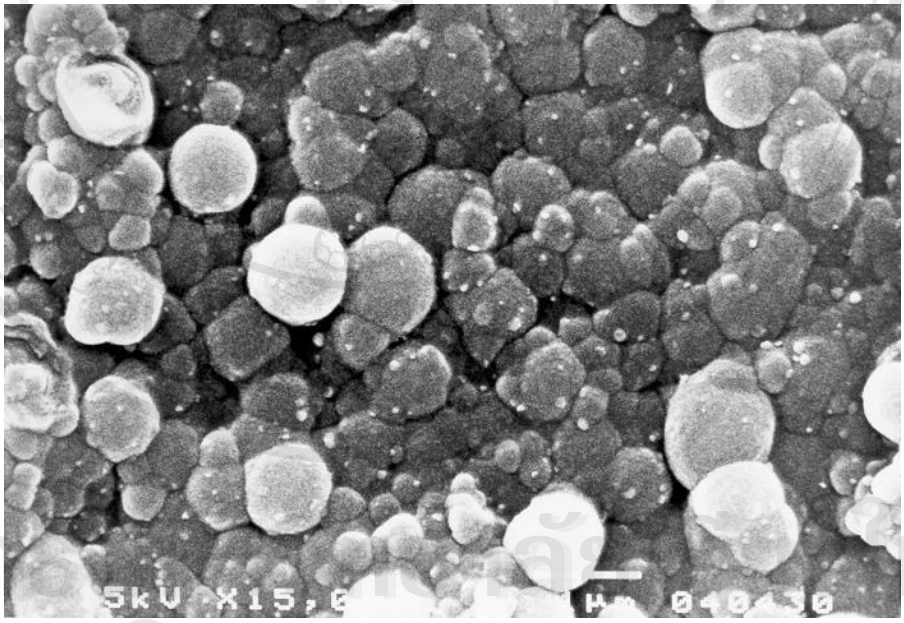

(d)

Figure 4.18 SEM micrographs of MJ12 with (a) 1000 K (b) 1100 K (c) 1200 K and (d) 1300 K nitridation in 10 $cm^3.s^{-1}$ NH_3 and carburization in 0.05 $cm^3.s^{-1}$ C_2H_2.

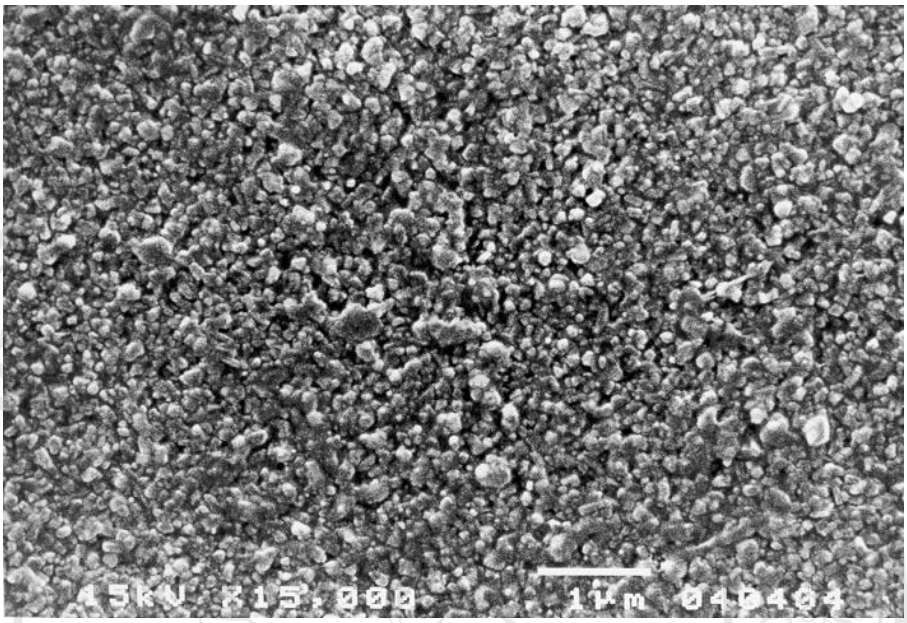

(a)

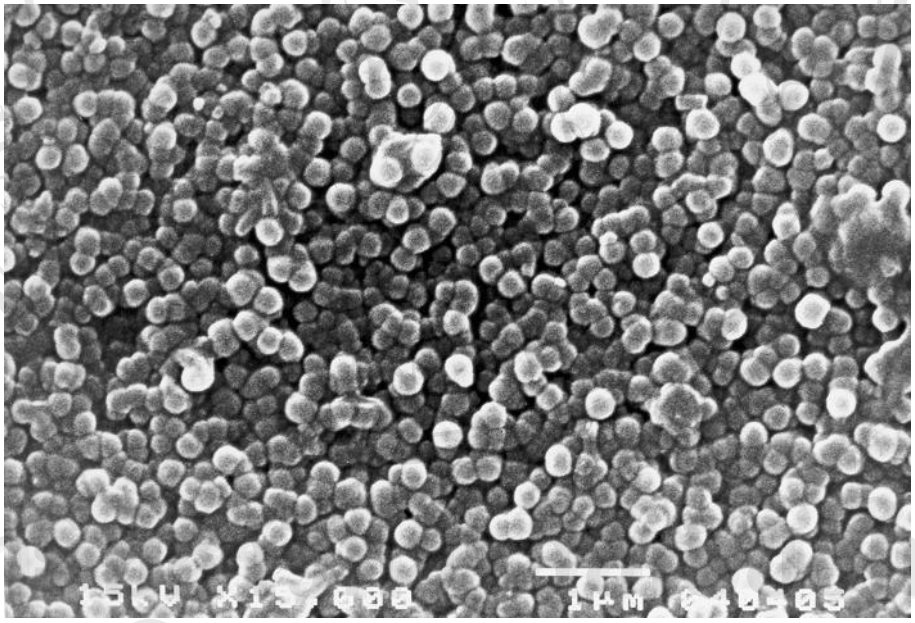

(b)

(Figure is continued to next page.)

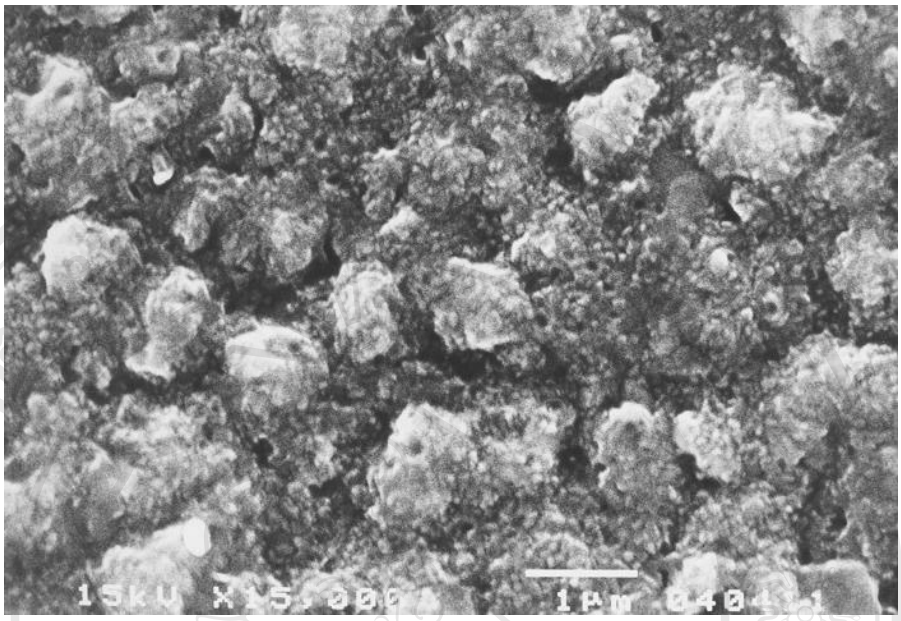

(c)

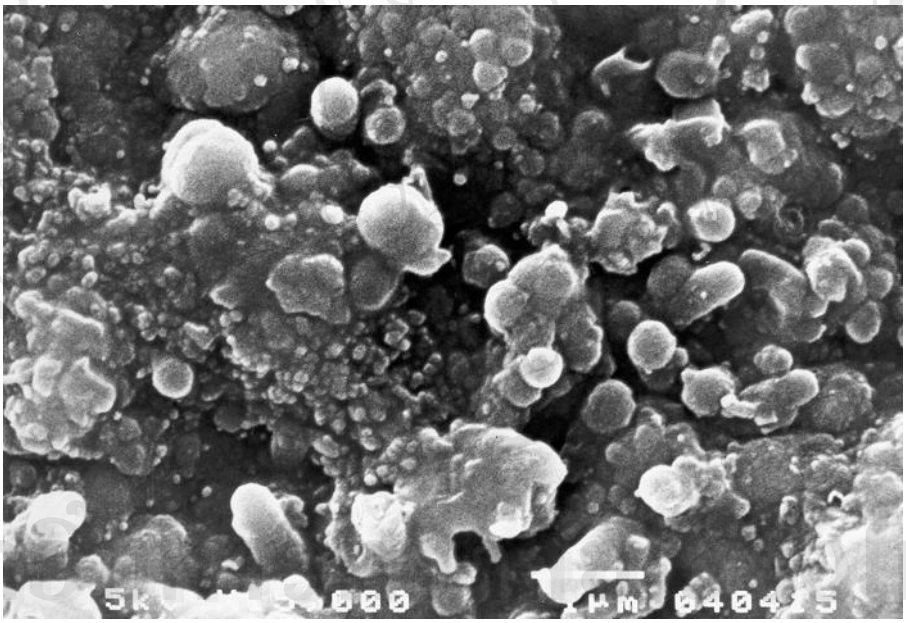

(d)

Figure 4.19 SEM micrographs of MJ47 with (a) 1000 K (b) 1100 K (c) 1200 K and (d) 1300 K nitridation in 10 $cm^3.s^{-1}$ NH_3 and carburization in 0.05 $cm^3.s^{-1}$ C_2H_2.

4.6.2 Nitridation by Direct Metal-Gas Reaction

Figure 4.20 and Figure 4.21 show the SEM micrographs of the alloys with 1000-1300 K nitridation. Irregular shape and flake-liked particles formed on the surface of the alloys nitrided at 1000-1300 K. Needle-liked particles formed only on the surface of the alloys nitrided at low temperature. At high temperature nitridation, size of the particles was larger than that at low temperature nitridation. Agglomerations form into large grains which could reflect the film density.

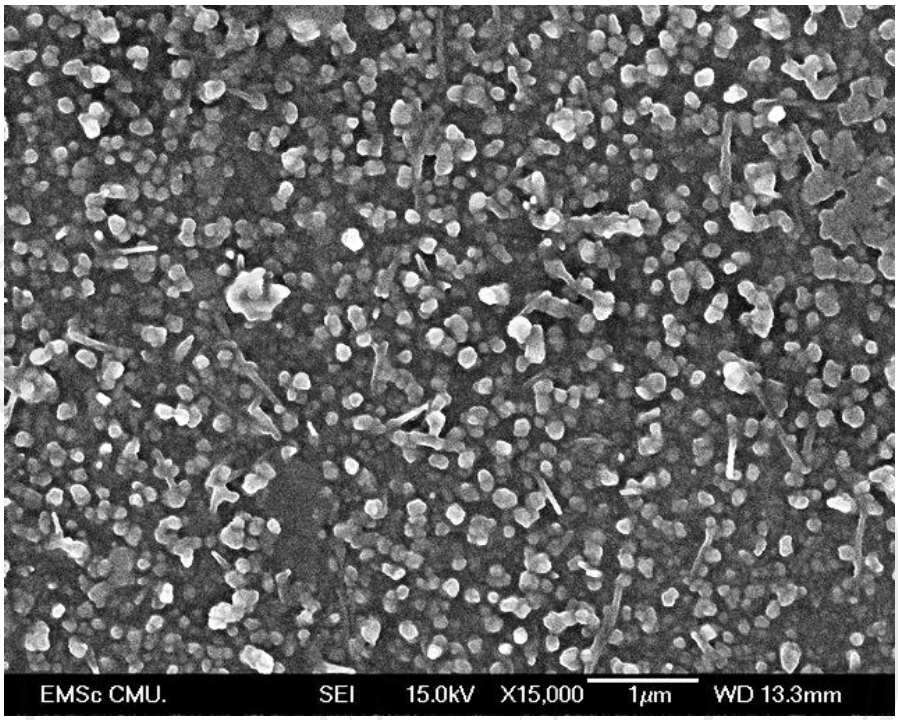

(a)

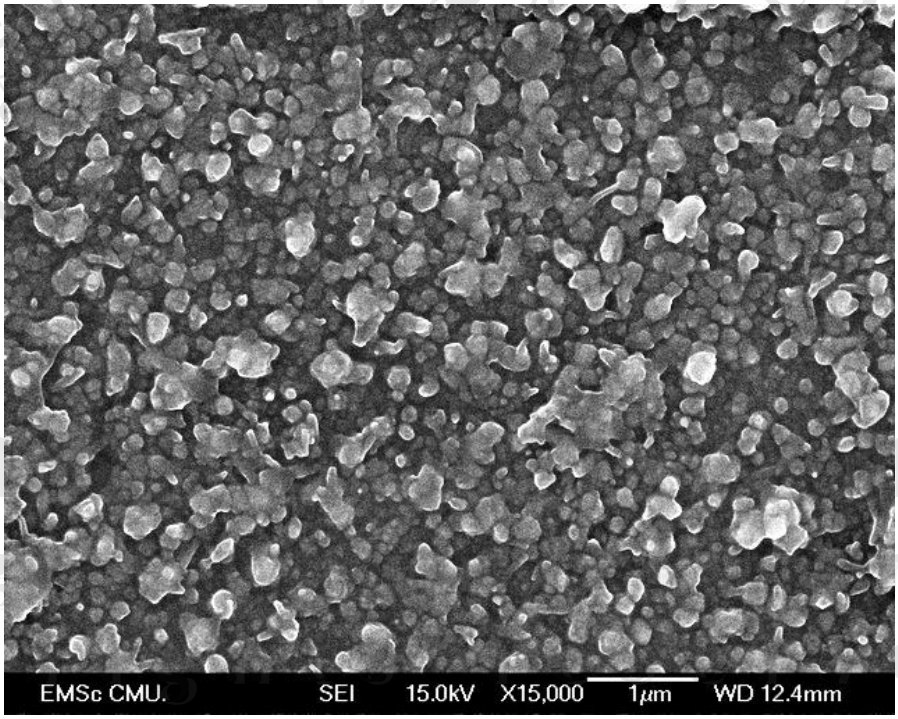

(b)

(Figure is continued to next page.)

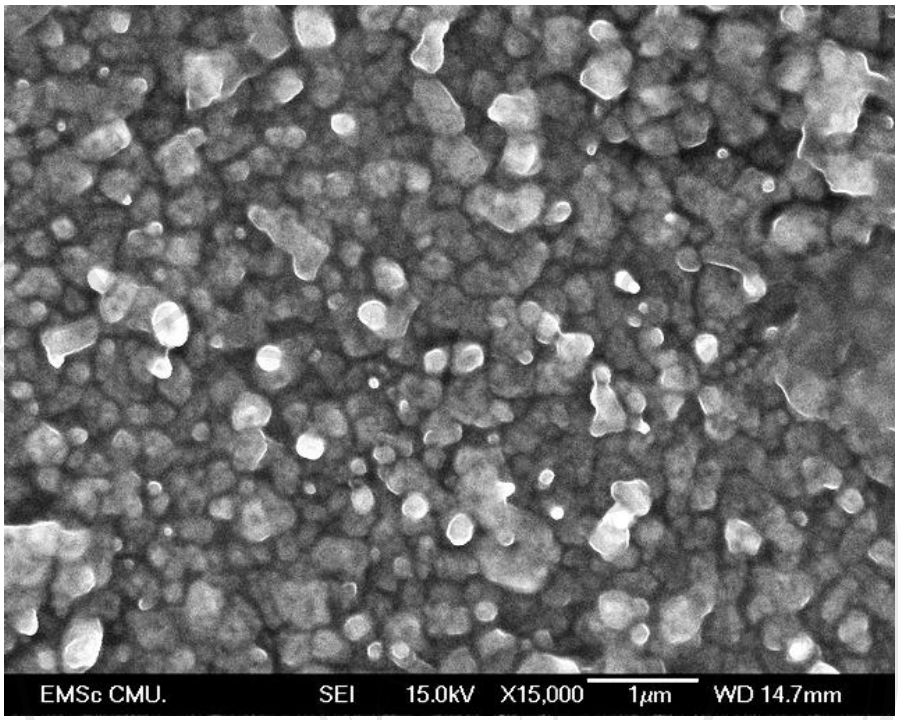

(c)

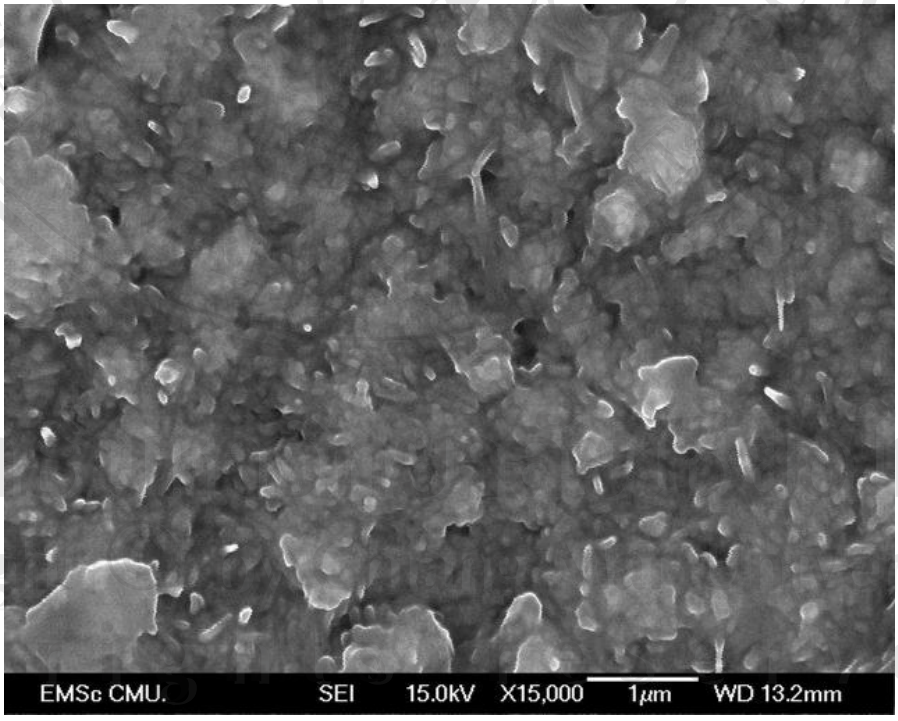

(d)

Figure 4.20 SEM micrographs of MJ12 with (a) 1000 K (b) 1100 K (c) 1200 K and (d) 1300 K nitridation in 10 $cm^3.s^{-1}$ NH_3.

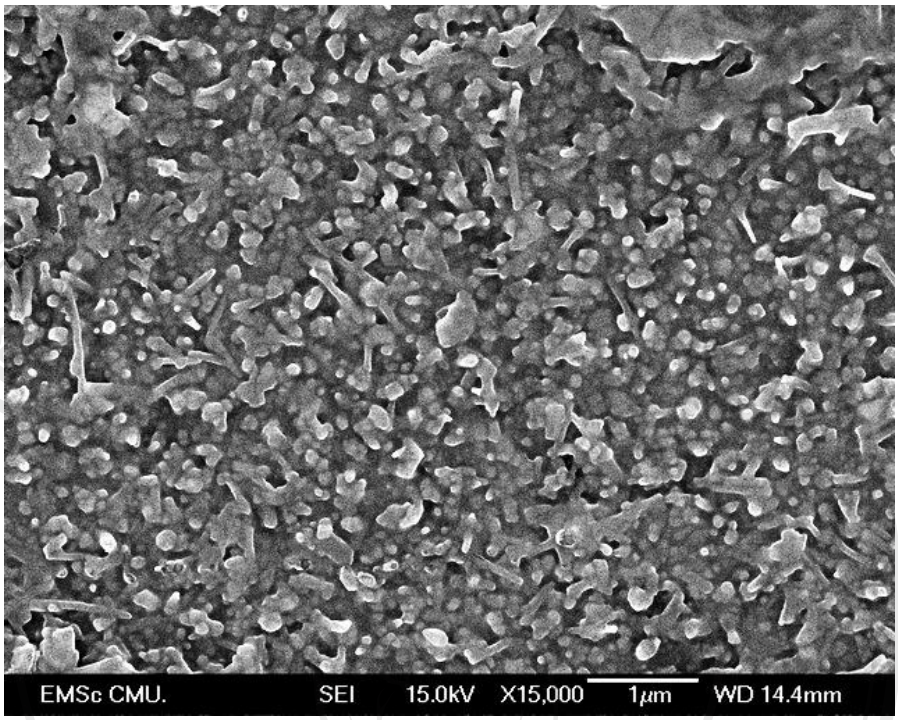

(a)

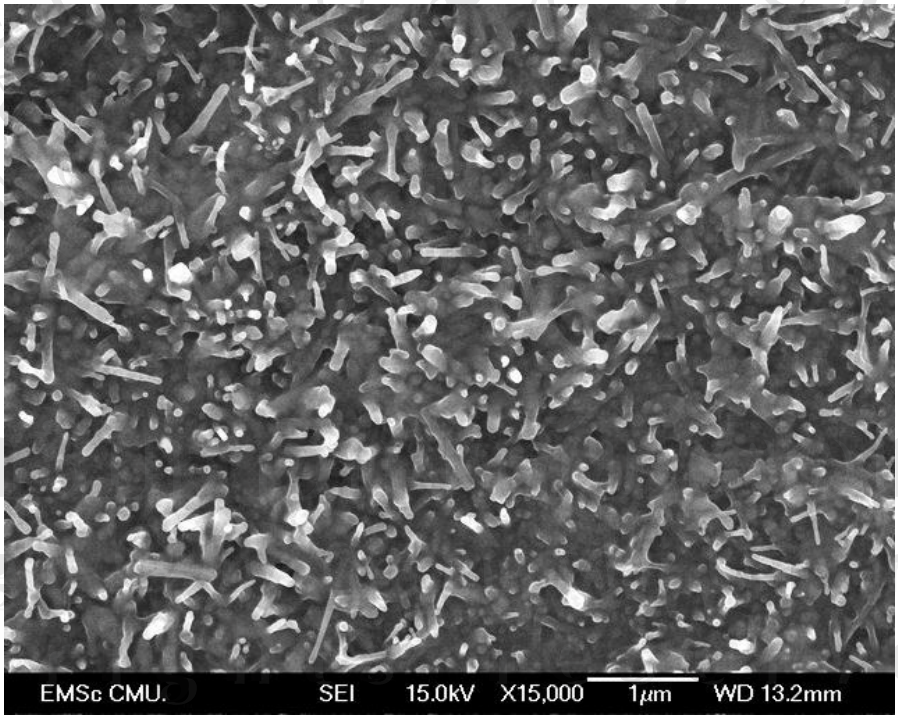

(b)

(Figure is continued to next page.)

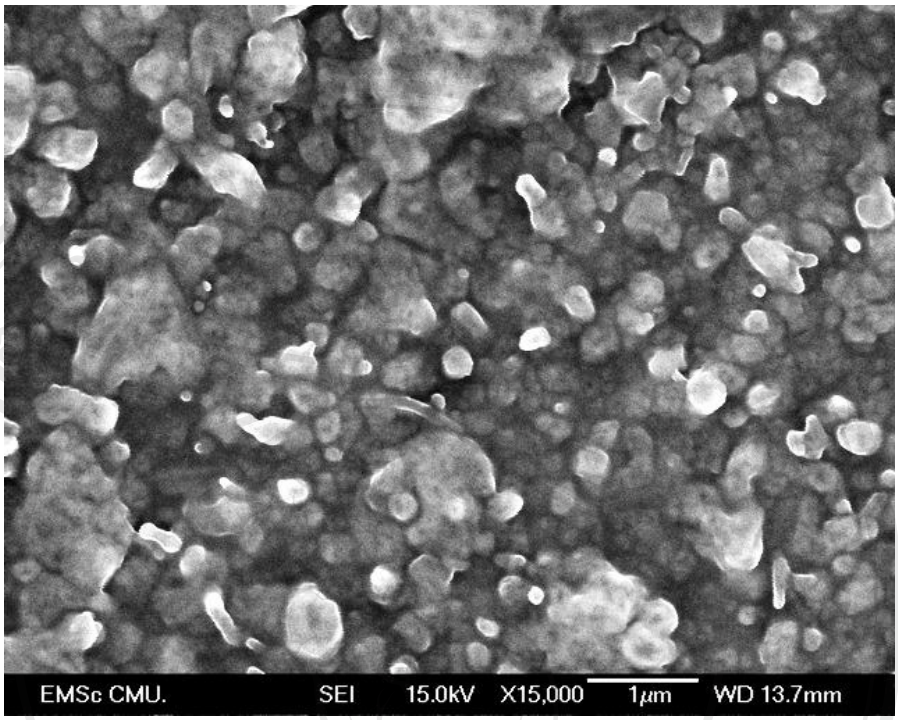

(c)

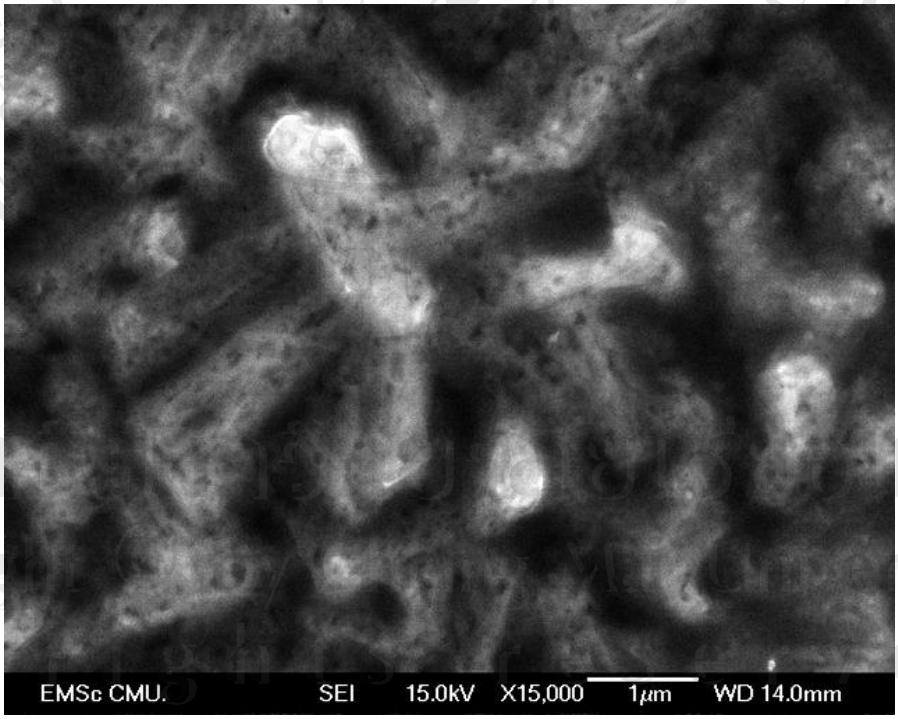

(d)

Figure 4.21 SEM micrographs of MJ47 with (a) 1000 K (b) 1100 K (c) 1200 K and (d) 1300 K nitridation in 10 $cm^3.s^{-1}$ NH_3.

4.6.3 Carburization by Directly Applying Voltages

SEM micrographs of the alloys after carburization are shown in Figure 4.22. There are irregular shape and flake-liked particles on the surface of both alloys. Needle-liked particles form on only MJ12. The particle on MJ12 is smaller than that on MJ47. Different carburization temperature can reflect the surface morphologies and properties.

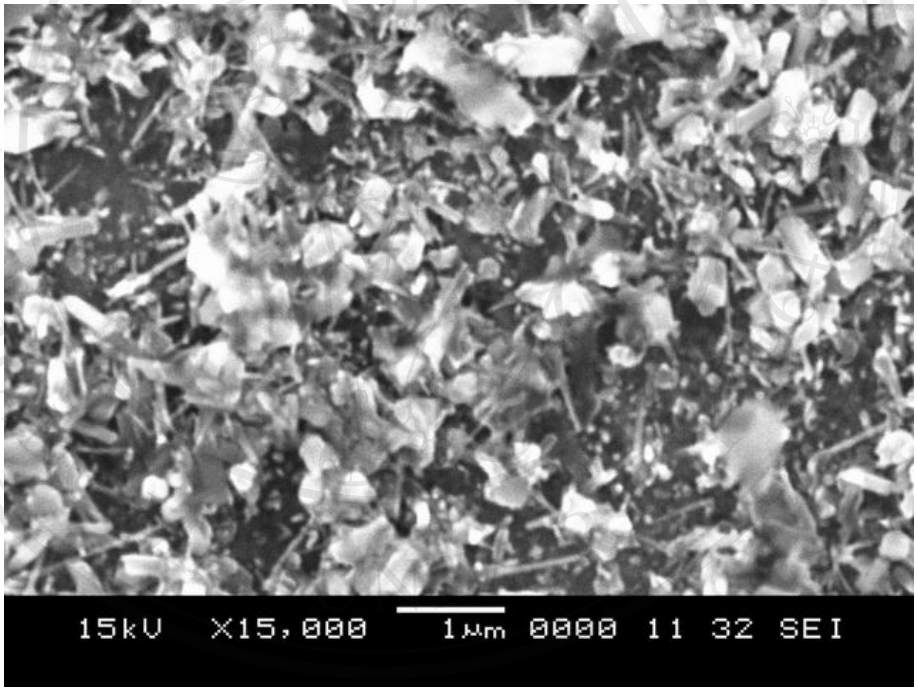

(a)

(Figure is continued to next page.)

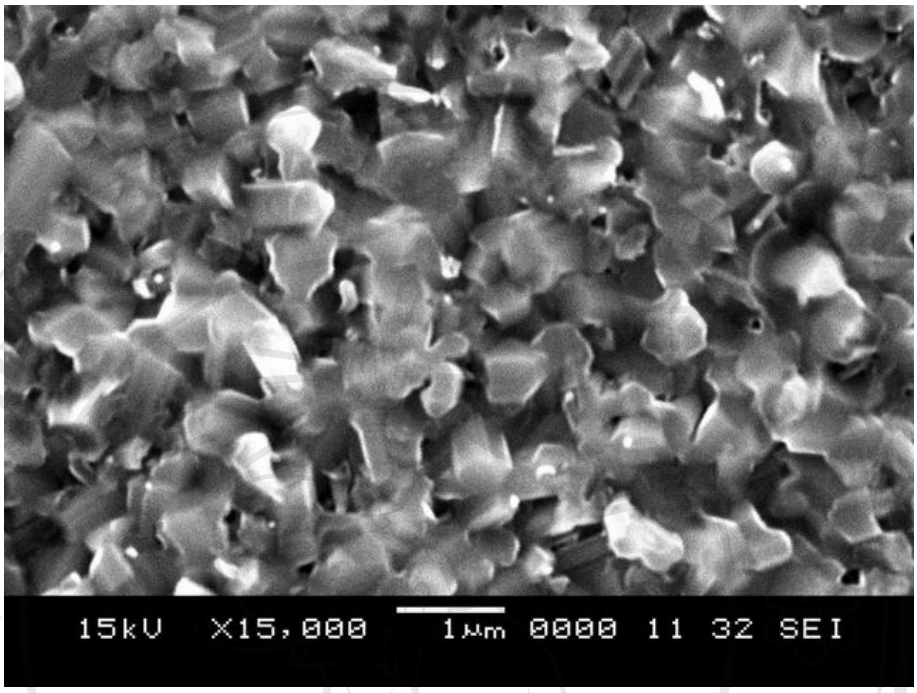

(b)

Figure 4.22 SEM micrographs of (a) MJ12 and (b) MJ47 after carburization by directly applying voltages.

4.7 Microhardness Test

4.7.1 Nitridation and Carburization by Direct Metal-Gas Reaction

Knoop hardness of the alloys with 1000-1300 K nitridation and carburization is shown in Figure 4.23. The Knoop hardness of as-received MJ12 and MJ47 are 332.1 ± 37.9 and 401.3 ± 28.4 kg.mm^{-2}, respectively. The Knoop hardness of MJ12 and MJ47 with 1000 K nitridation in 10 cm^3.s^{-1} NH_3 and carburization in 0.01 cm^3.s^{-1} C_2H_2 is 396.4 ± 20.7 and 447.1 ± 31.8 kg.mm^{-2}, respectively. It is evident that the Knoop hardness was improved although low C_2H_2 potential and coating temperature were used. The Knoop hardness values increased with increase of C_2H_2 potential and coating temperature due to the increase of carbide, carbonitride and nitride concentrations. The Knoop hardness values of MJ12 and MJ47 with 1300 K nitridation in 10 cm^3.s^{-1} NH_3 and carburization in 0.05 cm^3.s^{-1} C_2H_2 are maximum at 962.2 ± 87.8 and 992.4 ± 79.6 kg.mm^{-2}, respectively.

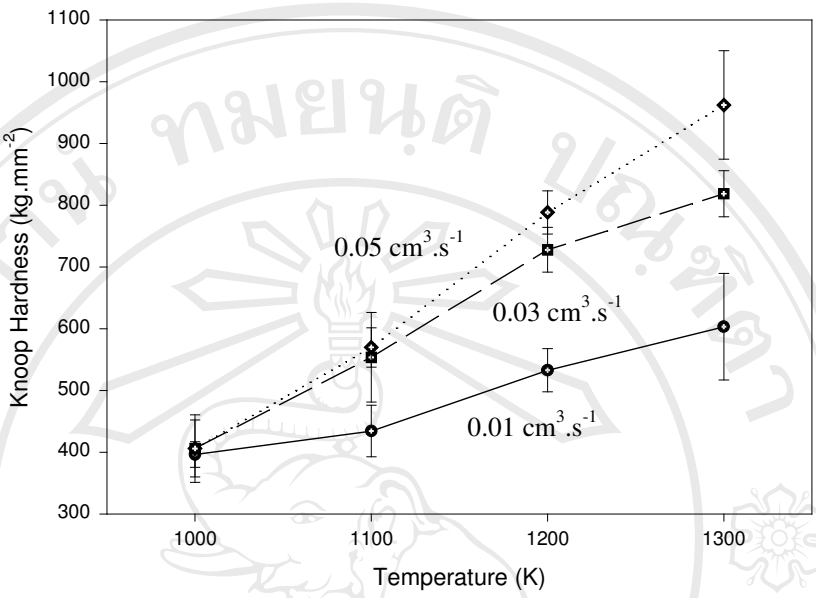

(a)

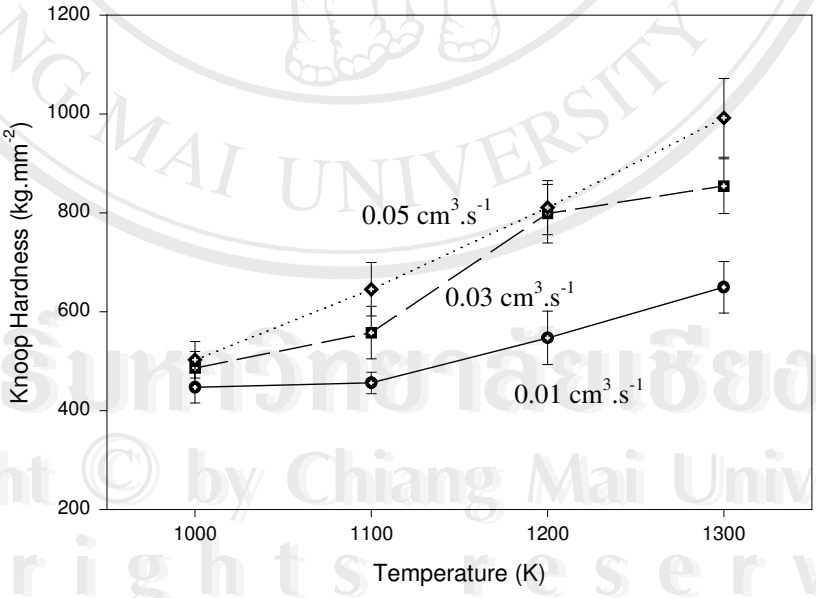

(b)

Figure 4.23 Knoop hardness of (a) MJ12 and (b) MJ47 nitrided in 10 $cm^3.s^{-1}$ NH_3 and carburized in 0.01, 0.03 and 0.05 $cm^3.s^{-1}$ C_2H_2.

4.7.2 Nitridation by Direct Metal-Gas Reaction

Knoop hardness of the alloys with 1000-1300 K nitridation are given in Figure 4.24. The Knoop hardness values increased with the increase in nitridation temperature. Film thickness and density of the alloys nitrided at low temperature are small. The indenter could penetrate through the film. The hardness value of the substrate influence on the hardness values of the alloys nitrided at low temperature. Their Knoop hardness values are so closed to those of the as-received alloys. At high temperature, film thickness, density and nitride concentration of the alloys are higher. The scale of these alloys can resist against the penetration of the indenter better than the scale nitrided at low temperature. Therefore, Knoop hardness values are higher than those at low temperature. The Knoop hardness values of MJ12 and MJ47 with 1300 K nitridation are at the maximum at 549.6±66.0 and 553.1±60.9 $kg.mm^{-2}$, respectively.

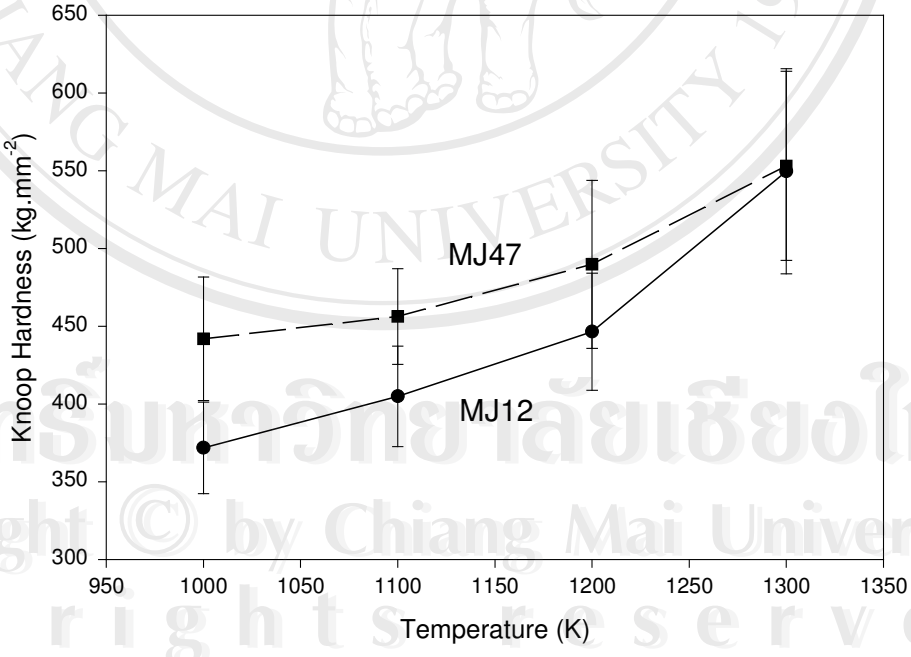

Figure 4.24 The Knoop hardness of MJ12 and MJ47 with 1000-1300 K nitridation.

4.7.3 Carburization by Directly Applying Voltages

After carburization, the Knoop hardness values of MJ12 and MJ47 are 360.9 ± 38.0 and 547.3 ± 34.5 $kg.mm^{-2}$, respectively. The Knoop hardness value of MJ47 is higher than that of MJ12 owing to their film density. Comparing to the as-received alloys, Knoop hardness value of the carburized MJ47 was increased at the higher rate than that of MJ12.

4.8 Wear Test

4.8.1 Nitridation and Carburization by Direct Metal-Gas Reaction

Wear rates of MJ12 and MJ47 with and without nitridation and carburization are given in Table 4.8. The results show the great improvement of the wear resistance of the nitrided and carbided alloys. The wear rates of the alloys which were nitrided and carburized by using 0.03 and 0.05 $cm^3.s^{-1}$ C_2H_2 are almost the same value. But for 0.01 $cm^3.s^{-1}$ C_2H_2, it is slightly higher than the two. Carbon potential is low; therefore, carbide concentration and solid carbon deposition are rather low. The hardness and the carbon lubrication for 0.01 $cm^3.s^{-1}$ C_2H_2 was low, resulting in low wear resistance in comparison with those of carburized in 0.03 and 0.05 $cm^3.s^{-1}$ C_2H_2. Furthermore, the sharp-edge particles on the alloys with nitridation and carburization using 0.01 $cm^3.s^{-1}$ C_2H_2 flow rate seems to reflect the wear rate comparing with the round-edge particles produced by using 0.05 $cm^3.s^{-1}$ C_2H_2 flow rate.

The wear rates should decrease with increase in nitridation and carburization temperature due to increase in nitride, carbide and carbonitride precipitation and solid carbon. The increase in hardness of the materials could make it become more brittle. The brittle materials can produce more wear debris, resulting in high wear rate. The irregularity of the wear rates is the compromise among these parameters.

Table 4.8 Wear rates of the alloys without and with nitridation and carburization at high temperature.

Alloys	Temperature (K)	Wear rate ($\times 10^{-8}$ $mm^3.mm^{-1}$)		
		At 0.01 $cm^3.s^{-1}$ C_2H_2	At 0.03 $cm^3.s^{-1}$ C_2H_2	At 0.05 $cm^3.s^{-1}$ C_2H_2
MJ12	As-received	214.48±14.00	214.48±14.00	214.48±14.00
	1000	3.92±0.49	3.19±0.84	3.37±0.79
	1100	9.03±1.48	2.74±0.93	1.69±0.49
	1200	3.03±0.38	6.24±1.51	0.81±0.36
	1300	4.61±0.46	1.64±0.64	2.14±0.35
MJ47	As-received	210.89±15.00	210.89±15.00	210.89±15.00
	1000	7.91±1.79	2.93±0.95	3.09±0.79
	1100	1.57±0.28	2.31±6.20	1.20±0.76
	1200	6.32±1.18	1.74±0.59	2.26±0.80
	1300	10.52±1.46	2.19±0.51	2.20±0.66

4.8.2 Nitridation by Direct Metal-Gas Reaction

The wear rates of the alloys with 1000-1300 K nitridation are shown in Figure 4.25. The wear rates decreased with increasing nitridation temperature due to the increase in hardness of the alloys. The wear rates of MJ12 and MJ47 with 1,300 K nitridation are minimum at $1.81 \pm 0.68 \times 10^{-8}$ and $1.60 \pm 0.28 \times 10^{-8}$ $mm^3.mm^{-1}$, respectively. Generally, hardness of TiN is lower than that of TiC [11]. This causes TiN to be less brittle and more difficult to fracture and spall than TiC.

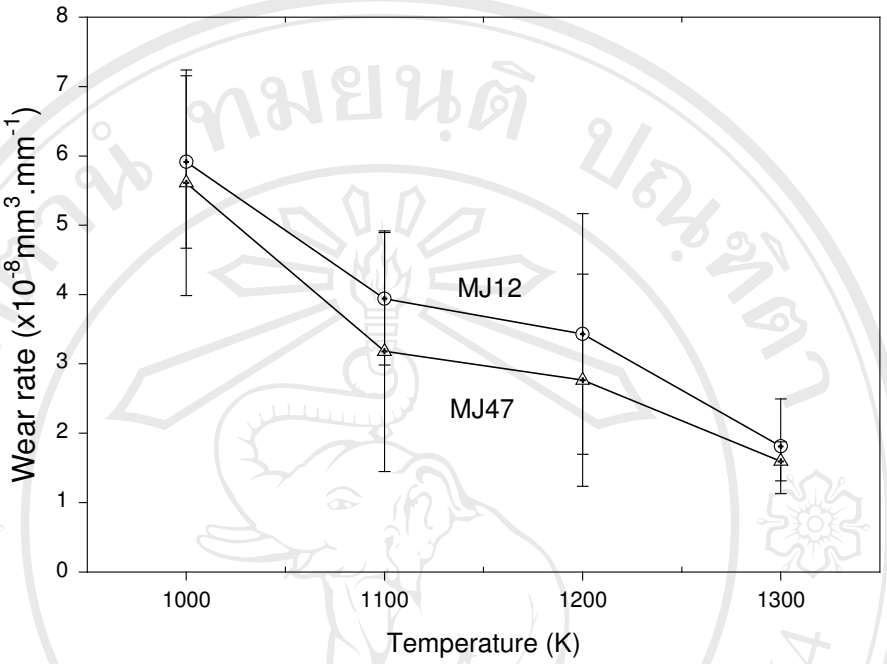

Figure 4.25 The wear rates of MJ12 and MJ47 with 1000-1300 K nitridation.

4.8.3 Carburization by Directly Applying Voltages

The wear rates of MJ12 and MJ47 carburized by using applied voltages are $4.17 \pm 1.47 \times 10^{-8}$ and $3.03 \pm 0.69 \times 10^{-8}$ $mm^3.mm^{-1}$, respectively. The wear rates of MJ47 with and without carburization are lower than those of MJ12 owing to their higher hardness. Comparing the two as-received alloys, MJ47 shows better wear resistance than MJ12. TiB_2 particles dispersed in the matrix of MJ47 is beneficial to improve wear resistance [5].